NPS ARCHIVE
1998.03
JERAULD, J.

DUDLEY KNOX LIBRARY
NAVAL POSTGRADUATE SCHOOL
MONTEREY CA 93943-5101

NAVAL POSTGRADUATE SCHOOL
Monterey, California

THESIS

ACOUSTICAL EMISSION SOURCE LOCATION IN THIN RODS THROUGH WAVELET DETAIL CROSSCORRELATION

by

Joseph G. Jerauld

March 1998

Thesis Advisor: Edward M. Wu

Approved for public release; distribution is unlimited.

DUDLEY KNOX LIBRARY
NAVAL POSTGRADUATE SCHOOL
MONTEREY CA 93943-5101

REPORT DOCUMENTATION PAGE

Form Approved OMB No. 0704-0188

Public reporting burden for this collection of information is estimated to average 1 hour per response, including the time for reviewing instruction, searching existing data sources, gathering and maintaining the data needed, and completing and reviewing the collection of information. Send comments regarding this burden estimate or any other aspect of this collection of information, including suggestions for reducing this burden, to Washington headquarters Services, Directorate for Information Operations and Reports, 1215 Jefferson Davis Highway, Suite 1204, Arlington, VA 22202-4302, and to the Office of Management and Budget, Paperwork Reduction Project (0704-0188) Washington DC 20503.

1. AGENCY USE ONLY *(Leave blank)*	2. REPORT DATE	3. REPORT TYPE AND DATES COVERED
	March 1998	Engineer's Thesis

4. TITLE AND SUBTITLE
ACOUSTICAL EMISSION SOURCE LOCATION IN THIN RODS THROUGH WAVELET DETAIL CROSSCORRELATION

5. FUNDING NUMBERS
Grant No. 32384-EG

6. AUTHOR(S)
Jerauld, Joseph G.

7. PERFORMING ORGANIZATION NAME(S) AND ADDRESS(ES)
Naval Postgraduate School
Monterey, CA 93943-5000

8. PERFORMING ORGANIZATION REPORT NUMBER

9. SPONSORING / MONITORING AGENCY NAME(S) AND ADDRESS(ES)
Engineering and Environmental Science Division
Army Research Office

10. SPONSORING/ MONITORING AGENCY REPORT NUMBER

11. SUPPLEMENTARY NOTES
The views expressed in this thesis are those of the author and do not reflect the official policy or position of the Department of Defense or the U.S. Government.

12a. DISTRIBUTION / AVAILABILITY STATEMENT
Approved for public release; distribution is unlimited.

12b. DISTRIBUTION CODE

13. ABSTRACT *(maximum 200 words)*

Flaws in structural elements release strain energy in the form of stress waves that can be detected through acoustical emission techniques. The transient nature of a stress wave is analytically inconsistent to Fourier Transforms, and the wave characteristics under the effects of dispersion and attenuation deviate from the formal basis of the Windowed Fourier Transform. The transient solid body elastic waves contain multiple wave types and frequency components which lend themselves to the time and frequency characteristics of Wavelet Analysis. Software implementation now enables the exploration of the Wavelet Transform to identify the time of arrival of stress wave signals for source location in homogeneous and composite materials. This investigation quantifies the accuracy and resolution of two existing source location methods and develops a third technique using the Discrete Wavelet Transform on a windowed portion of the stress wave signal. A refined method for the spatial location of material damage induced stress waves can be used to directly monitor the safe-life of structures and provide a quantitative measure for the risk assessment of critical and aging structures. This investigation was partially supported by the Army Research Office.

14. SUBJECT TERMS

15. NUMBER OF PAGES
151

16. PRICE CODE

17. SECURITY CLASSIFICATION OF REPORT	18. SECURITY CLASSIFICATION OF THIS PAGE	19. SECURITY CLASSIFI- CATION OF ABSTRACT	20. LIMITATION OF ABSTRACT
Unclassified	Unclassified	Unclassified	UL

NSN 7540-01-280-5500

Standard Form 298 (Rev. 2-89)
Prescribed by ANSI Std. 239-18

DUDLEY KNOX LIBRARY
NAVAL POSTGRADUATE SCHOOL
MONTEREY, CA 93943-5101

Approved for public release; distribution is unlimited

ACOUSTICAL EMISSION SOURCE LOCATION IN THIN RODS THROUGH WAVELET DETAIL CROSSCORRELATION

Joseph G. Jerauld
Lieutenant Commander, United States Navy
B.S., California Polytechnic State University, June 1986
M.S., Naval Postgraduate School, September 1997

Submitted in partial fulfillment of the
requirements for the degree of

AERONAUTICAL AND ASTRONAUTICAL ENGINEER

from the

NAVAL POSTGRADUATE SCHOOL
March 1998

DUDLEY KNOX LIBRARY
NAVAL POSTGRADUATE SCHOOL
MONTEREY CA 93943-5101

ABSTRACT

Flaws in structural elements release strain energy in the form of stress waves that can be detected through acoustical emission techniques. The transient nature of a stress wave is analytically inconsistent to Fourier Transforms, and the wave characteristics under the effects of dispersion and attenuation deviate from the formal basis of the Windowed Fourier Transform. The transient solid body elastic waves contain multiple wave types and frequency components which lend themselves to the time and frequency characteristics of Wavelet Analysis. Software implementation now enables the exploration of the Wavelet Transform to identify the time of arrival of stress wave signals for source location in homogeneous and composite materials. This investigation quantifies the accuracy and resolution of two existing source location methods and develops a third technique using the Discrete Wavelet Transform on a windowed portion of the stress wave signal. A refined method for the spatial location of material damage induced stress waves can be used to directly monitor the safe-life of structures and provide a quantitative measure for the risk assessment of critical and aging structures. This investigation was partially supported by the Army Research Office.

DISCLAIMER

The views expressed in this thesis are those of the author and do not reflect the official policy or position of the Department of Defense of the U.S. Government.

Readers are also cautioned that the computer code in this thesis may not have been exercised for all cases of interest. While effort has been made, within the time available, to ensure that the program is free of computational and logical errors, additional verification should be applied. The use of this application is at the risk of the user.

TABLE OF CONTENTS

I. INTRODUCTION 1
A. DAMAGE DETECTION AND FAILURE SITE LOCATION 1
B. SIGNAL ANALYSIS OF STRESS WAVES 2
C. SOURCE LOCATION TECHNIQUES 3
II. WAVE EQUATIONS IN GENERAL ANISOTROPIC SOLIDS 5
A. EQUATIONS OF MOTION 5
B. ONE DIMENSIONAL WAVE PROPAGATION IN ANISOTROPIC SOLIDS 9
III. SOURCE LOCATION TECHNIQUES 13
A. CHARACTERISTICS OF TRANSIENT SIGNAL ANALYSIS TECHNIQUES 13
B. THRESHOLD CROSSING 15
C. GAUSSIAN CROSS CORRELATION 18
D. WAVELET DETAIL CROSS CORRELATION 19
IV. EXPERIMENTAL SETUP 29
A. OBJECTIVE AND SCOPE 29
B. EQUIPMENT 29
C. TEST SIGNALS 30
V. EXPERIMENTAL RESULTS 37
A. LARGE (3/8 IN.) STEEL ROD 37
B. SMALL (1/8 IN.) STEEL ROD 46
C. CARBON FIBER ROD 52
VI. CONCLUSIONS AND RECOMMENDATIONS 59
A. CONCLUSIONS 59
B. RECOMMENDATIONS 60
APPENDIX A. REPRESENTATIVE SIGNALS FROM THE TEST RODS 63
APPENDIX B. LOCATION AND BEST CORRELATION LEVEL HISTOGRAMS. 89
APPENDIX C. EXPERIMENTAL METHODS 125
APPENDIX D. MATLAB SCRIPT FILES 129
A. WAVEDETXCORR.M 129
B. WAVDETCORSTAT.M 130
C. SIGNAL_PLOTTER.M 131
LIST OF REFERENCES 135
INITIAL DISTRIBUTION LIST 137

ACKNOWLEDGEMENT

I wish to thank my wife Lisa and my children Benjamin and Audrey for their support, patience and understanding during the conduct of this investigation. I would like to thank my advisor, Professor Ed Wu, for his guidance, intuition, and musical taste and for occasionally kicking me. As Vince Lombardi said, "The quality of a man's life is directly proportional to his commitment to excellence, no matter his field of endeavor."

I. INTRODUCTION

A. DAMAGE DETECTION AND FAILURE SITE LOCATION

In the design of aircraft and space structures, there is a requirement for high performance and low weight. As the designer estimates the loads and stresses, the classical approach is to use a factor of safety to ensure reliability and safety. Except for very simple structures, neither the service load (or load history) can be well defined, nor the methodology for calculating the limiting failure load well established. The ratio of calculated failure load to service load, or the calculated failure life to desired service life are utilized as safety factors. The magnitude of this factor of safety is often based on judgment and experience vice quantitative parameters. The ability of structural designers to maximize the strength to weight or stiffness to weight ratios is bounded by the safety factor and produces structures that are designed heavier and bulkier than the operating loads require to preclude catastrophic failure. Higher performance can be achieved if the structure is designed closer to operational load levels. Safety and reliability can still be assured if there is a system to monitor, detect and locate the onset of damage. In both metal and composite structures, flaws ultimately leading to failure begin at sizes which can easily escape current detection techniques. The small size of these initial failures enables them to be statistically spread throughout the structure, but spatial clustering can lead to catastrophic failure. Dislocations, cracks, delaminations, and fiber breakage all can lead to the failure of a structure. These point failures release strain energy which creates stress waves in the structure. Acoustical emission techniques detect stress waves by the particle motion that they create in the material itself. Most current source location techniques require operator input to calculate the source location for each signal, and do not calculate locations in real time. A large number of test signals must be made in order to accurately determine the location distributions for a given location method. To facilitate the processing of these signals, a method of determining the acoustic emission

source location that is free of continuous operator intervention is required for applications. An automated or semi-automated technique is more suitable for applications in aircraft or other high performance structures. Such a technique could be used by inflight data recorders and processing to warn aircrew of potential structural failure, or alert ground personnel to the locations for inspection and repair.

Alternately, the reliability of a structure may be assured by proof testing. Structural elements that pass proof testing are assumed to be safe at the operational load, when it may have transitioned to a less reliable state through the creation of new flaws in the proof testing process. With an effective damage detection and source location system, the element's worthiness at the operational load will be known. Risk of structural failure can be assessed based on information that is garnered from the structure. There can be a qualitative decision to inspect, repair or replace the structure of elements of the structure, or leave in service in the absence of any failures.

B. SIGNAL ANALYSIS OF STRESS WAVES

The localized failure site is analogous to the perturbation caused by a pebble in a still pond. On contact with the water surface, a transverse ripple wave is created on the surface. After the pebble penetrates the water surface, a compressive wave is created and propagates through the volume. An elastic solid under load is much the same. When a failure caused by a dislocation, a crack, or a fiber breaking in a composite occurs, the energy released propagates through the structure in the form of stress redistribution by elastic waves. There are two primary types of stress waves that propagate through the solid medium. When a solid medium is deformed, and released suddenly, both distortional, (shear deformation), and dilatational, (volume deformational), waves are produced. Particle motion parallel to the direction of propagation is characteristic of waves of dilatation, or longitudinal waves. Motion perpendicular to direction of propagation is representative of waves of distortion, or transverse waves. When a wave of either type impinges on a boundary of the solid, waves of both types will be generated

by the reflection (Kolsky, 1954). Structural materials are never perfectly elastic. The stress waves will attenuate, a loss in amplitude as it propagates through the medium, due to internal friction. Additionally, the stress waves do not exist as a single component of a single frequency. The many frequency components of both the longitudinal and transverse waves will each travel at different characteristic velocities through the solid. This phenomena is dispersion.

The critical parameter for determining the location of the source is the time of arrival of the wave, or a frequency component of that wave, at a sensor. Attenuation and dispersion affect the characteristics of the signal received at different sensors. The signals created by the stress waves are transitory, that is, the wave characteristics are different for different time or spatial windows. Fourier analysis transforms a stationary signal in the time domain to the frequency domain. The frequency spectrum, or presence of a frequency can be determined, but the time of arrival of that frequency cannot be resolved. Windowed Fourier transforms use a smaller but nevertheless fixed window, and evaluate the frequency content of the signal within that window. The transitory, non-stationary nature of the stress waves caused by the microscopic failure sites precludes the applicability of Fourier analysis. Wavelet signal processing techniques retain the time information that is lost in Fourier analysis. The signals are decomposed into a time-frequency basis that can determine the arrival and location of specific frequencies and transient phenomena. (Hess-Nielsen,1996)

C. SOURCE LOCATION TECHNIQUES

There are several methods which may be used to determine the time of arrival of a signal at a sensor, and each has strengths and limitations. The three degrees of freedom are amplitude, frequency, and time. Threshold Crossing, uses a preset level (voltage) as the time of arrival of the signal. When the signal strength reaches or exceeds this level, the time is marked, and a comparison is made to when the signal crossing that preset level at other sensors at different spatial locations. Gaussian Cross Correlation uses a

modulated cosine of one *a priori* selected frequency to determine the arrival time of the signal at a sensor. Correlation is carried out by sweeping (digitally) the modulated cosine pulse across the signals from each sensor, and the sum of the products of the two signals is calculated at each point. The peaks in the cross correlation functions correspond to the arrival of that frequency at the sensor (Ziola,1991). A third technique is explored in this investigation using Wavelet Detail Cross Correlation. A discrete wavelet transform is performed on the signals from each of the sensors. The reconstructed detail levels are then crosscorrelated to determine the difference in the time of arrivals at the sensors. A number of parameters were compared for the determination of location. The purpose of this investigation is to assess the feasibility of detecting the time of arrival of the acoustic emissions caused by the stress waves in homogeneous (steel) and heterogeneous composite (carbon fiber) rods, and to determine the location of the source of the acoustic emissions. Gish (1995) indicated a resolution to the location distribution on the order of the diameter of the sensing elements. This investigation is limited to one-dimensional cylindrical sample geometry of both homogeneous and composite materials. Steel and carbon fiber composite materials offer a wide range of varying propagation characteristics in attenuation and dispersion. They are chosen to broaden the applicability of the findings of this investigation. Only existing Wavelet Analysis methods are used, no new analytical techniques in the discrete wavelet transform are developed. Wave theory for thin rods is presented in Section II. The analytical bases for source location by threshold crossing, gaussian crosscorrelation, and wavelet detail crosscorrelation is described in detail in Section III. The experimental set up is given briefly in Section IV. The experimental results are given in Section V. Conclusions and recommendations are made in Section VI. Appendix A contains plots of representative signals, wavelet decompositions and crosscorrelations from the three test samples. Appendix B has the histograms of the location distributions, as well as the histograms of the best correlation level. Experimental method is given is greater detail in Appendix C. MATLAB script files written for the Wavelet Detail Cross Correlation and data analysis are given in Appendix D.

II. WAVE EQUATIONS IN GENERAL ANISOTROPIC SOLIDS

A. EQUATIONS OF MOTION

The set of governing equations for wave propagation in an isotropic solid is available in many text books of continuum - solid mechanics also in specialized books on stress waves. We develop herein the governing wave equations for homogeneous anisotropic solids for applications to composite materials.

For a general solid subjected to a time dependent surface traction $T_i^{\nu}(t)$, on a surface area A, with outward normal ν_j,(ν_j is taken to be independent of time for small deformation) at any instant, t, the *local* dynamic equilibrium between the external surface force and the internal stresses (σ_{ji}) adjacent to the surface is represented by the boundary condition:

$$T_i^{\upsilon}(t) = \sigma_{ji}(t)\nu_j . \qquad (1)$$

The *global* dynamic equilibrium for the entire body is maintained by summation of all the surface traction $T_i^{\nu}(t)$ on the external surface area A and the internal body forces within the internal volume to be balanced by the inertia force:

$$\int_A T_i^{\nu} dA + \int_V X_i dV = \rho \frac{d^2 x_i}{dt^2}, \qquad (2)$$

where X_i is field induced body force with dimension (wd) of [Force]/[Volume], ρ is the density wd [mass]/[Volume] and $\frac{d^2 x_i}{dt^2}$ is the acceleration in terms of the fixed inertia coordinates x_i (Eulerian coordinates). The boundary condition (1) is substituted into (2) and Divergence theorem applied (which must be in Lagrangian coordinates ξ_j, which moves with the body). Under the assumptions that density is time invariant, Equation (2) becomes:

$$\int_V \left(\frac{\partial \sigma_{ji}}{\partial \xi_j} + X_i - \rho \frac{d^2 x_i}{dt^2} \right) dV = 0$$

Assuming an arbitrary volume, then Newton's second law takes on a form in terms of the two different coordinate systems:

$$\frac{\partial \sigma_{ji}}{\partial \xi_j} + X_i = \rho \frac{d^2 x_i}{dt^2}. \tag{3}$$

The Eulerian coordinates x_i which are fixed with an inertia system are related to Lagrangian coordinates ξ_i (which moves with the body by displacements u_i) by the kinematics relation:

$$x_i = u_i + \xi_i. \tag{4}$$

The set of equations governing the dynamic behaviors of solid includes: the equations of motion, the displacement relating the Eulerian to the Lagrangian coordinates, the constitutive relation for materials responses between strain and stress, the kinematics relation between displacements and strain. Respectively, the set of governing equations are :

$$\frac{\partial \sigma_{ji}}{\partial \xi_j} + X_i = \rho \frac{d^2 x_i}{dt^2}, \tag{5a}$$

$$x_i = u_i + \xi_i, \tag{5b}$$

$$\sigma_{ij} = C_{ijpq} \varepsilon_{pq}, \tag{5c}$$

$$\varepsilon_{pq} = \frac{1}{2} \left(\frac{\partial u_p}{\partial \xi_q} + \frac{\partial u_q}{\partial \xi_p} \right). \tag{5d}$$

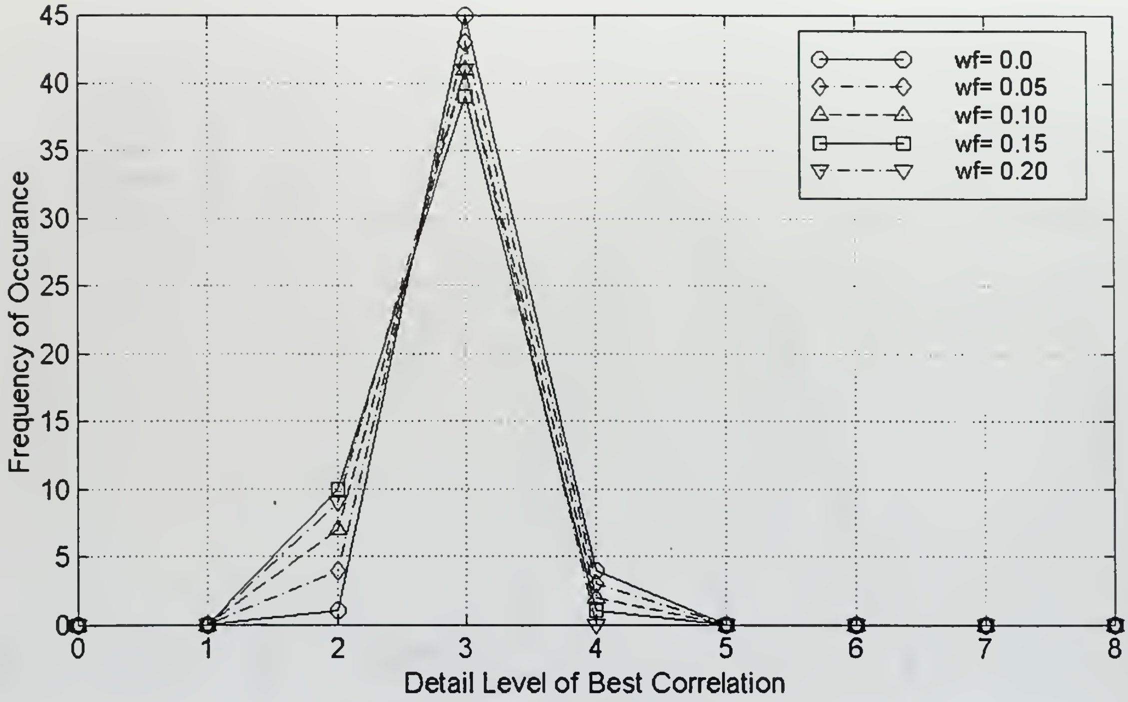

Figure B.15. Histogram of Detail Level of Best Crosscorrelation Large Steel Rod Signals 01 through 50, Sensors #1 and #3, min.(variance/max.), weighting factor = [0.0, 0.05, 0.10, 0.15, 0.20]

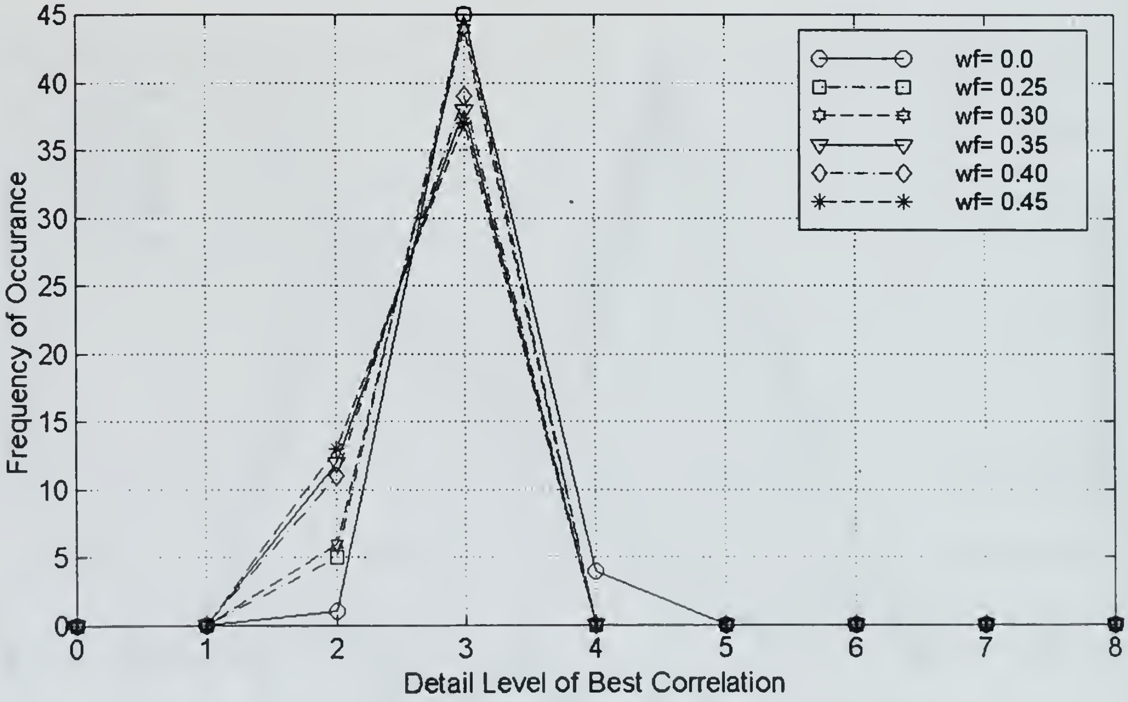

Figure B.16. Histogram of Detail Level of Best Crosscorrelation Large Steel Rod Signals 01 through 50, Sensors #1 and #3, min.(variance/max.), weighting factor = [0.0, 0.25, 0.30, 0.35, 0.40, 0.45]

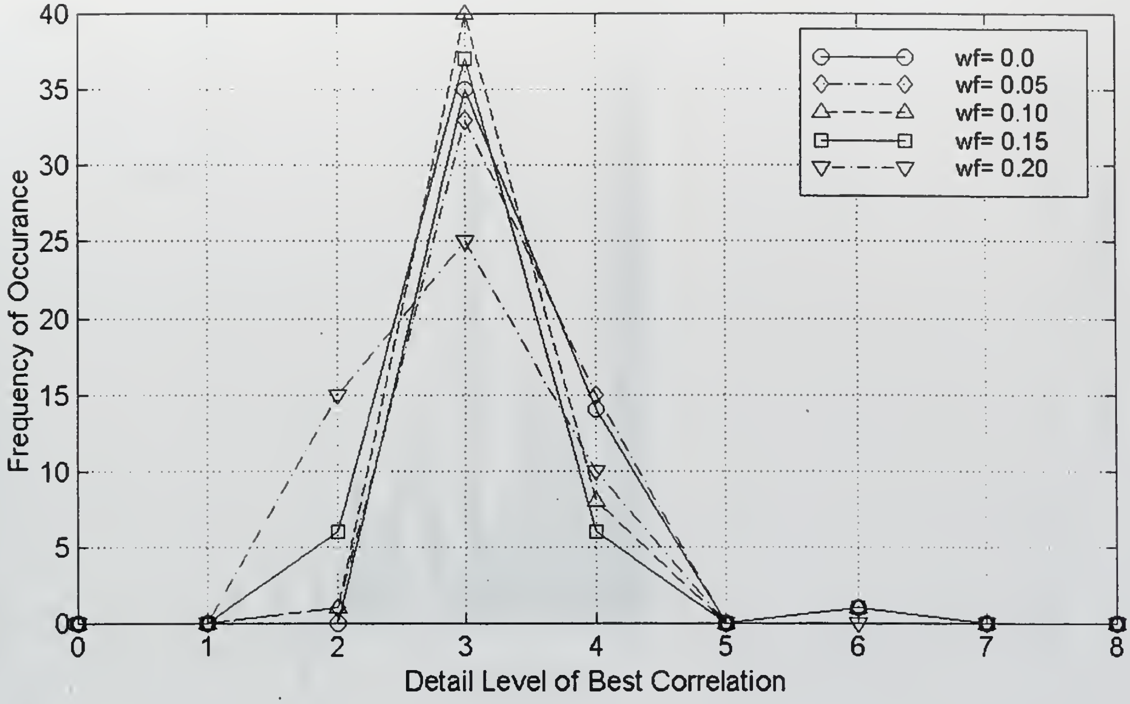

Figure B.17. Histogram of Detail Level of Best Crosscorrelation Large Steel Rod Signals 01 through 50, Sensors #1 and #4, min.(variance/max.), weighting factor = [0.0, 0.05, 0.10, 0.15, 0.20]

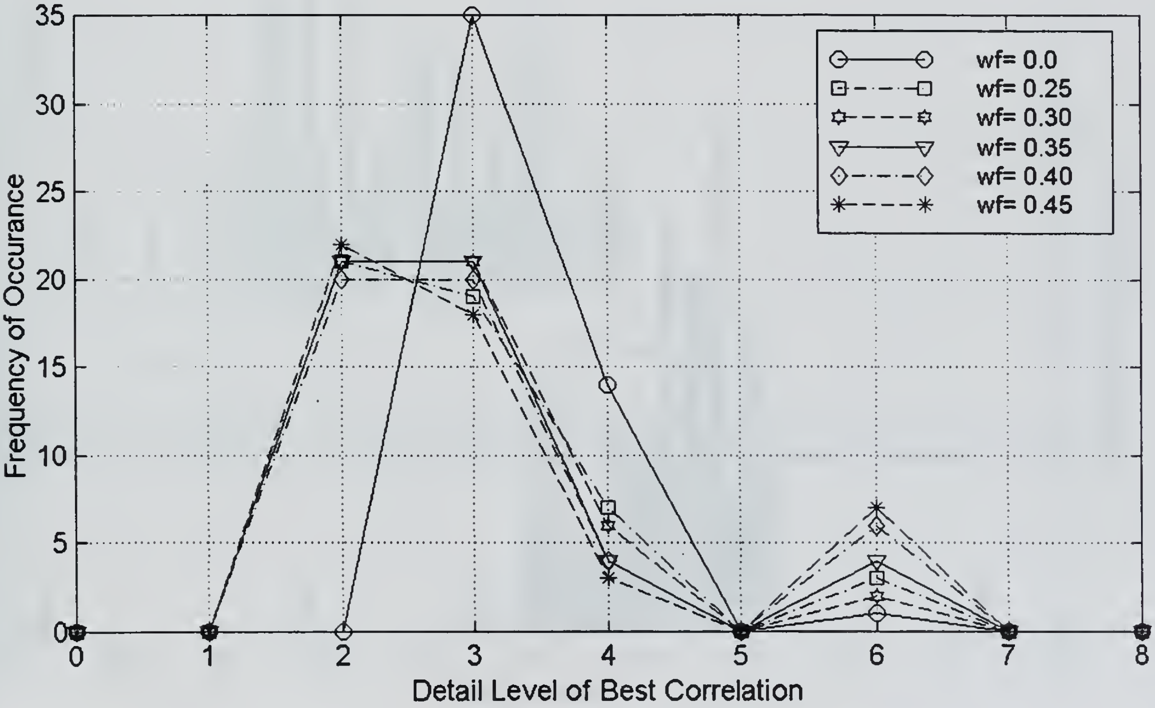

Figure B.18. Histogram of Detail Level of Best Crosscorrelation Large Steel Rod Signals 01 through 50, Sensors #1 and #4, min.(variance/max.), weighting factor = [0.0, 0.25, 0.30, 0.35, 0.40, 0.45]

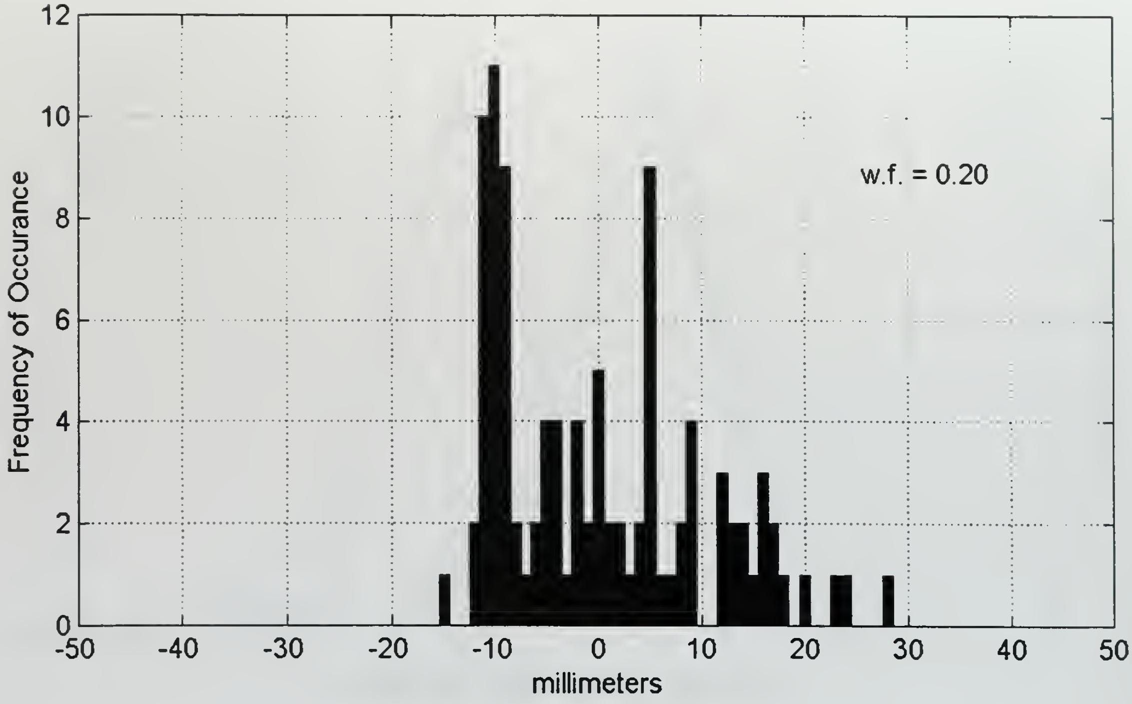

Figure B.19. Wavelet Detail Crosscorrelation Location Histogram for Large Steel Rod Sensors #1 and #2, Mean = -0.002 mm, Std Dev. = 10.115 mm, Transducer Diameter = 9.525 mm.

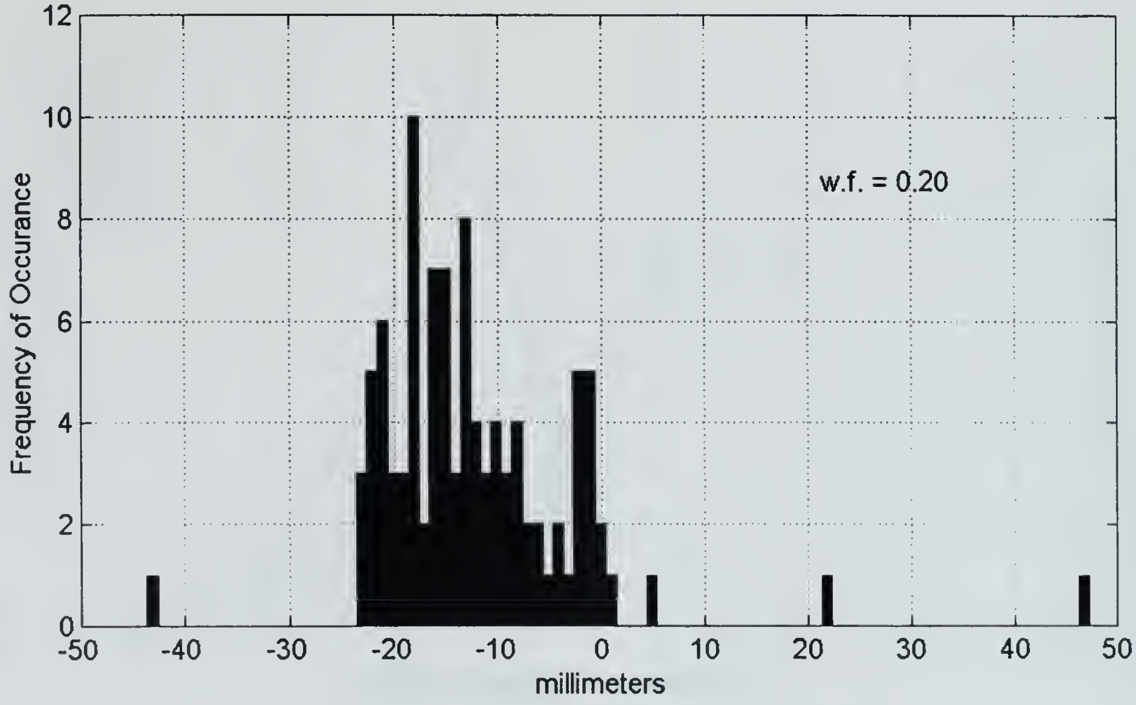

Figure B.20. Wavelet Detail Crosscorrelation Location Histogram for Large Steel Rod Sensors #1 and #3, Mean = -12.154 mm, Std Dev. = 10.206 mm, Transducer Diameter = 9.525 mm.

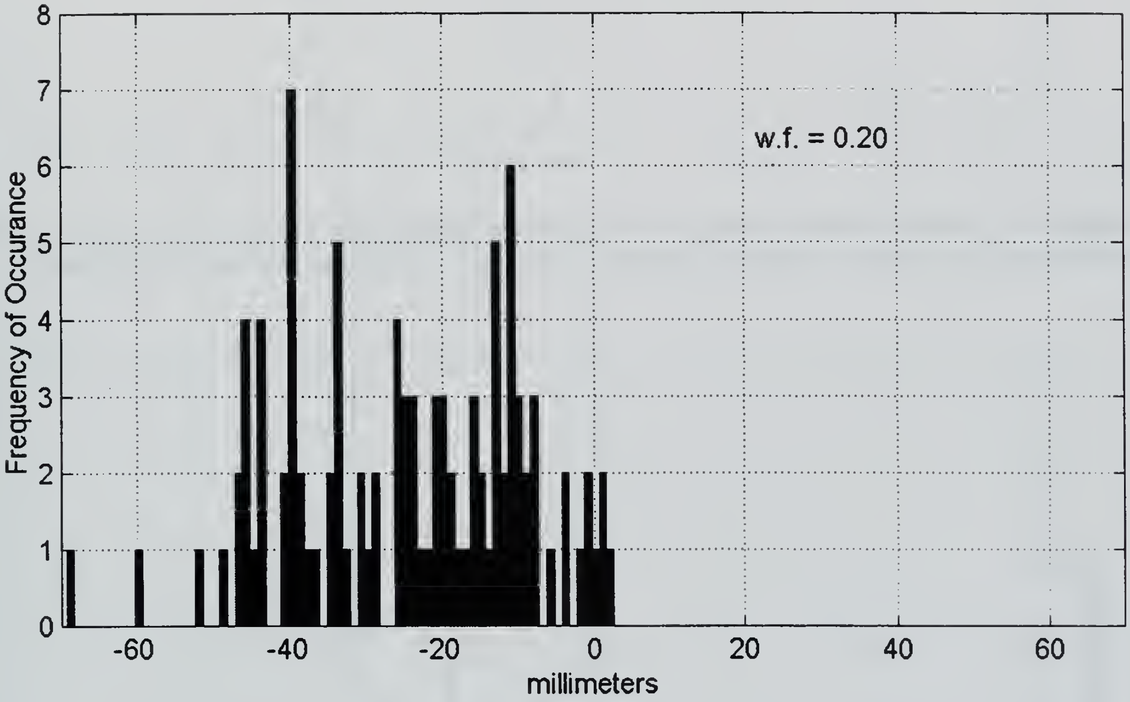

Figure B.21. Wavelet Detail Crosscorrelation Location Histogram for Large Steel Rod Sensors #1 and #4, Mean = -24.762 mm, Std Dev. = 15.405 mm, Transducer Diameter = 9.525 mm.

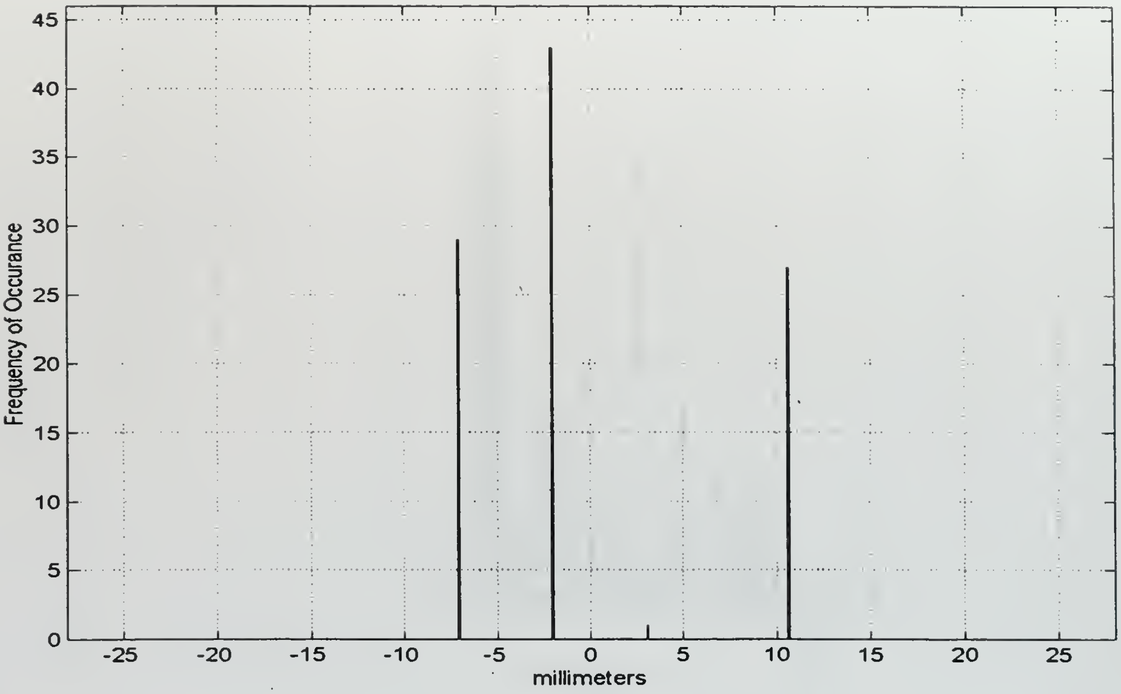

Figure B.22. Wavelet Detail Crosscorrelation Location Histogram for Large Steel Rod, Detail 3 max, Sensors #1 and #2, Mean = 0.006 mm, Std Dev. = 6.849 mm, Transducer Diameter = 9.525 mm.

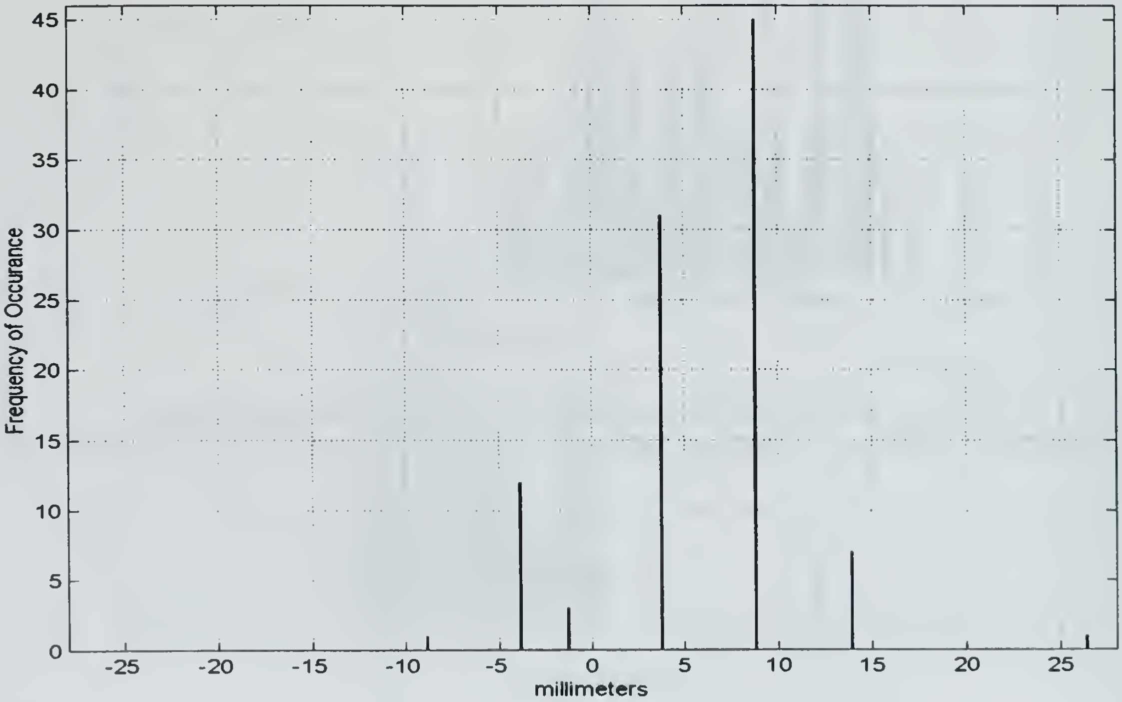

Figure B.23. Wavelet Detail Crosscorrelation Location Histogram for Large Steel Rod, Detail 3 max, Sensors #1 and #3, Mean = 5.780 mm, Std Dev. = 5.392 mm, Transducer Diameter = 9.525 mm.

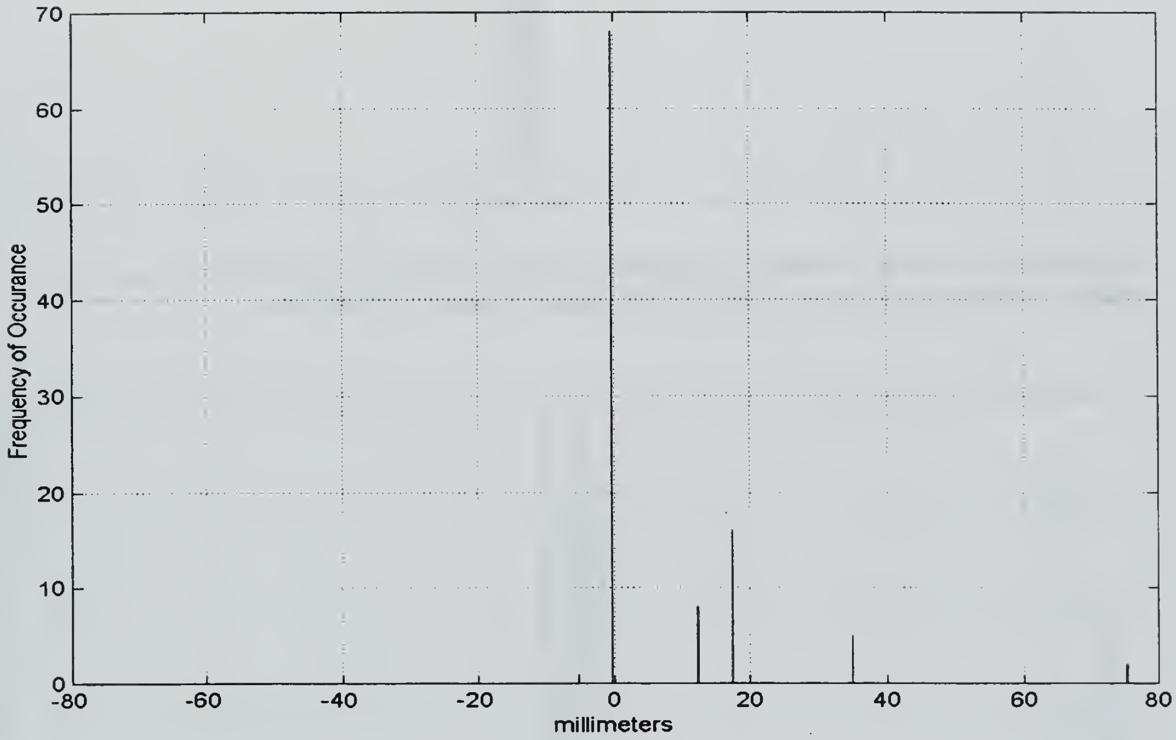

Figure B.24. Wavelet Detail Crosscorrelation Location Histogram for Large Steel Rod Detail 3 max, Sensors #1 and #4, Mean = 6.850 mm, Std Dev. = 13.823 mm, Transducer Diameter = 9.525 mm.

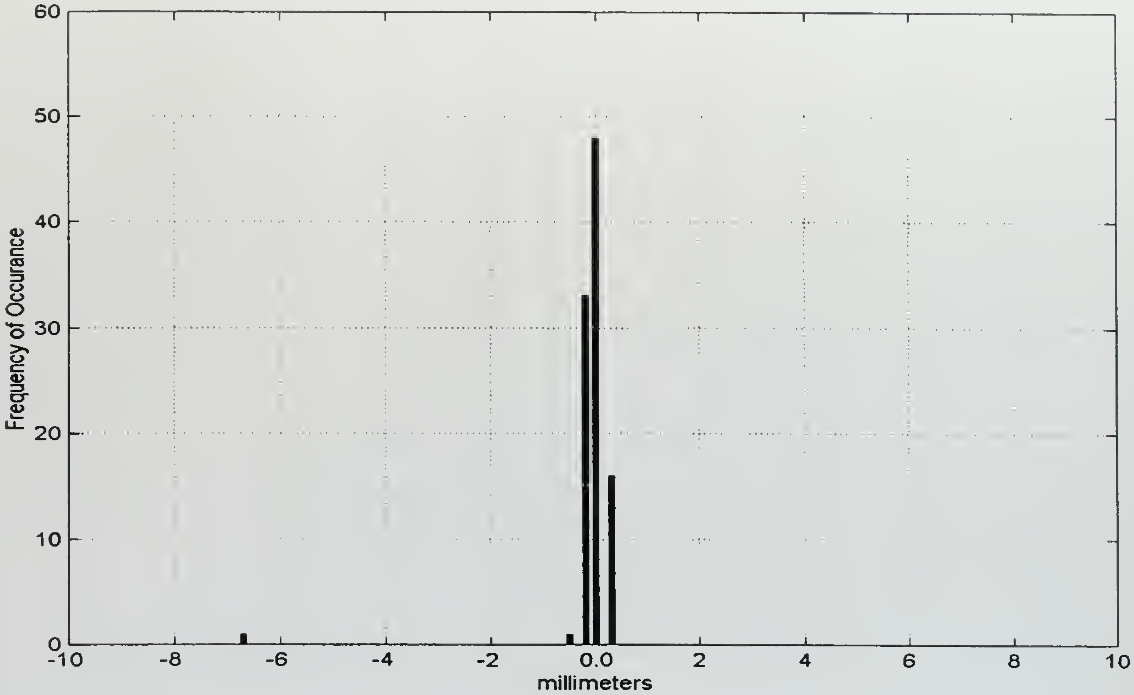

Figure B.25. Threshold Crossing Location Histogram for Small Steel Rod Sensors #1 and 2 Mean = -0.091 mm, Std Dev. = 0.693 mm, Transducer Diameter = 5.080 mm.

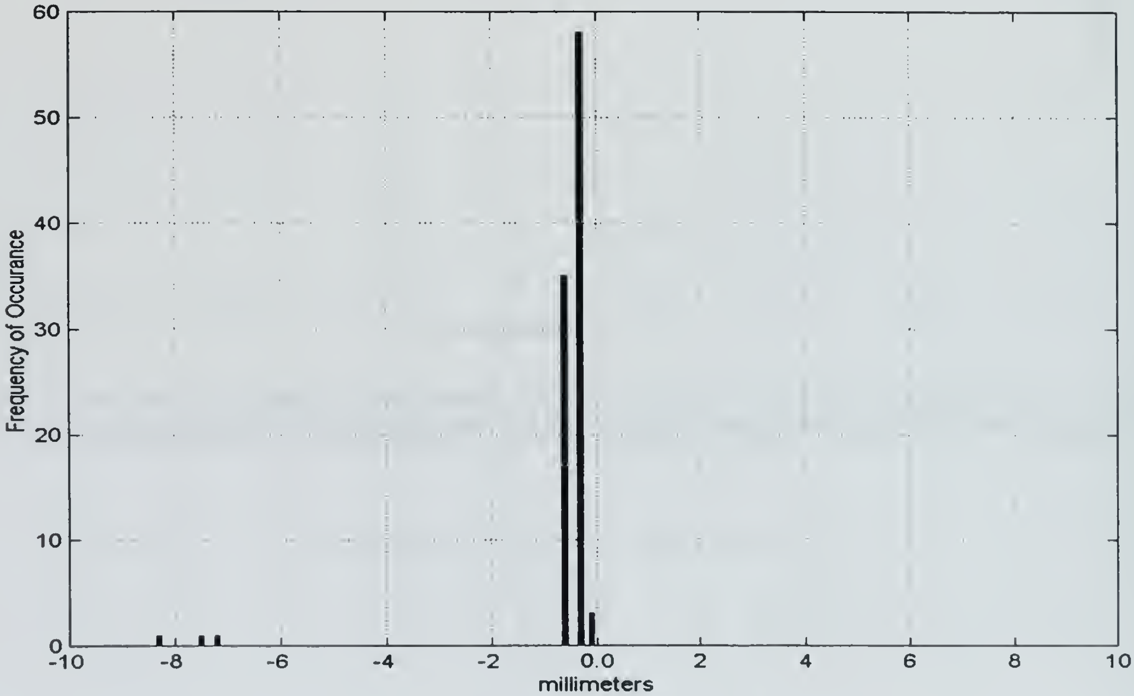

Figure B.26. Threshold Crossing Location Histogram for Small Steel Rod Sensors #1 and #3 Mean = -0.623 mm, Std Dev. = 1.263 mm, Transducer Diameter = 5.080 mm.

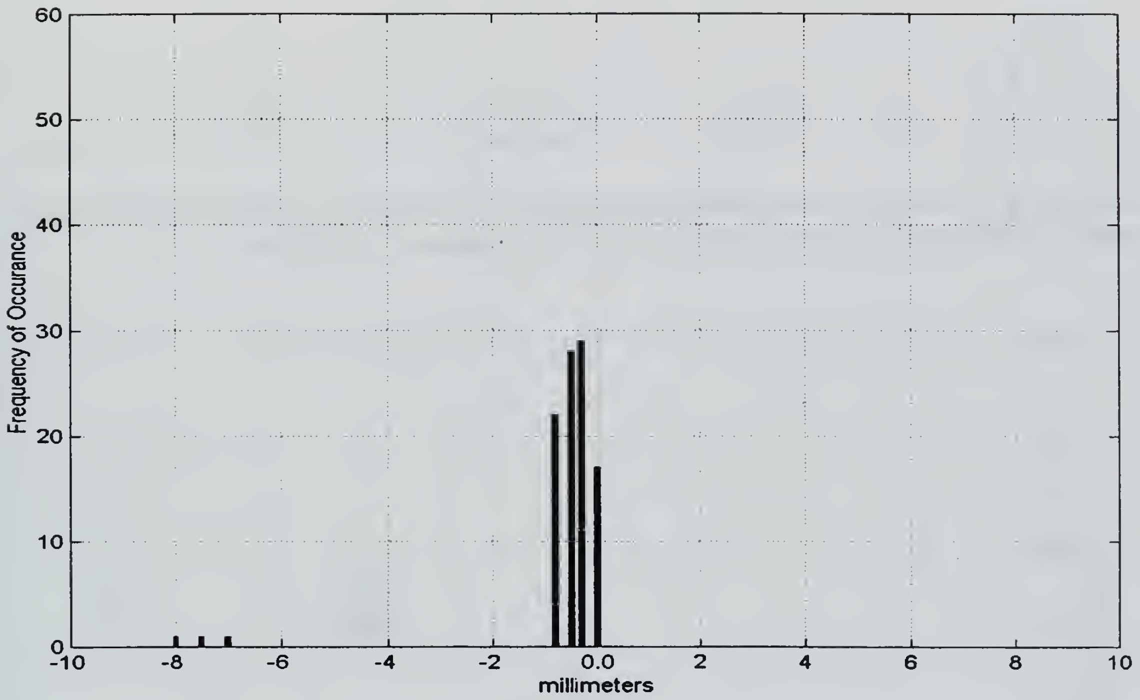

Figure B.27. Threshold Crossing Location Histogram for Small Steel Rod Sensors #1 and #4 Mean = -0.634 mm, Std Dev. = 1.250 mm, Transducer Diameter = 5.080 mm.

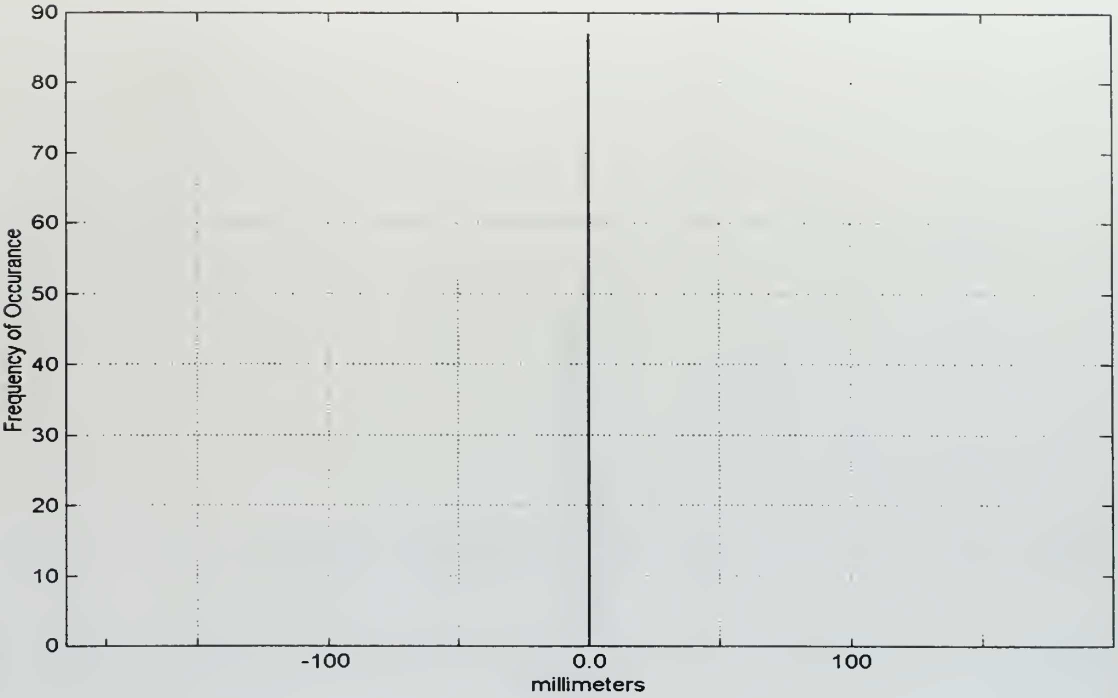

Figure B.28. Gaussian Crosscorrelation Location Histogram for Small Steel Rod Sensors #1 and #2 Mean = -1.869 mm, Std Dev. = 18.573 mm, Transducer Diameter = 5.080 mm.

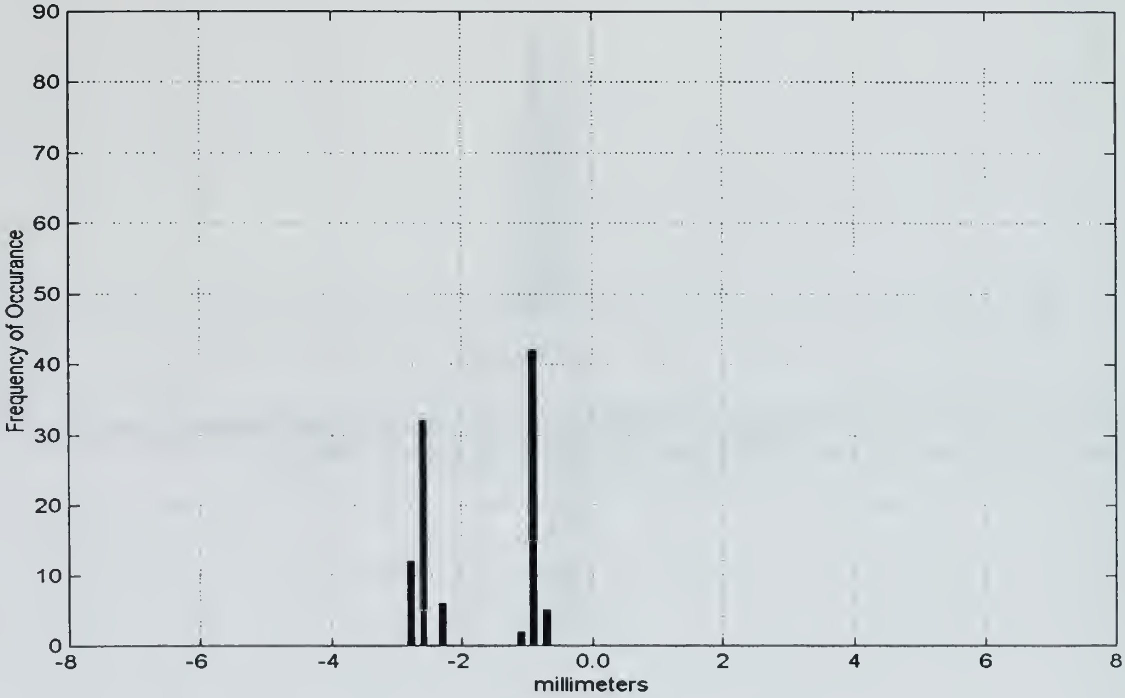

Figure B.29. Gaussian Crosscorrelation Location Histogram for Small Steel Rod Sensors #1 and #3 Mean = -1.759 mm, Std Dev. = 0.874 mm, Transducer Diameter =5.080 mm.

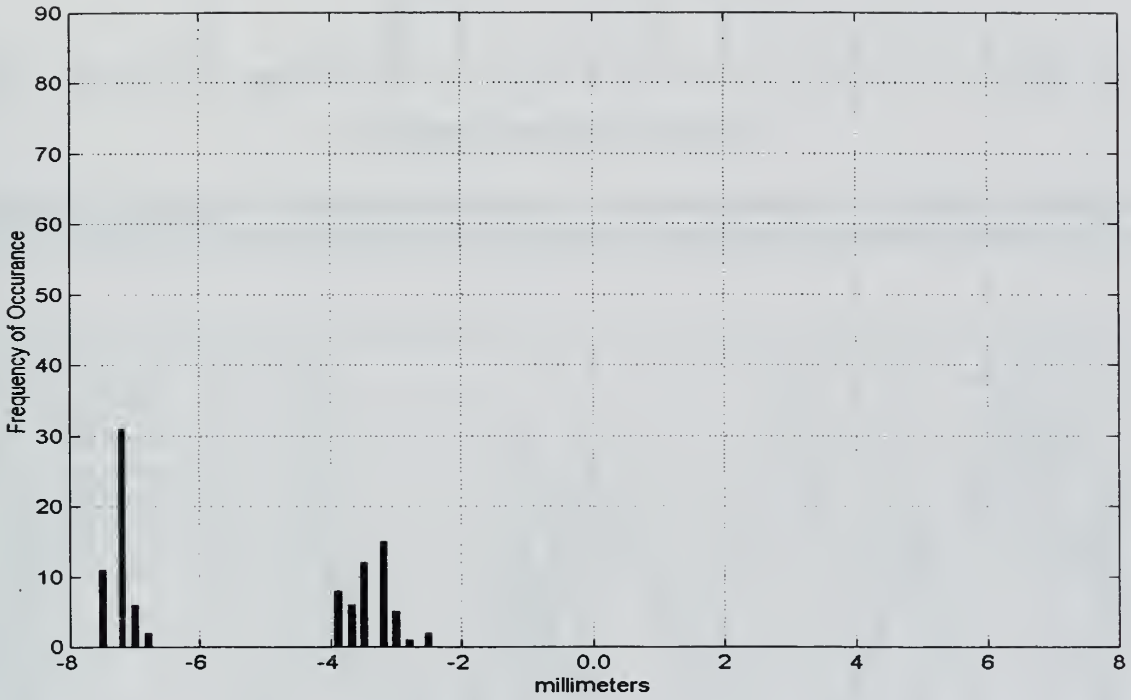

Figure B.30. Gaussian Crosscorrelation Location Histogram for Small Steel Rod Sensors #1 and #4 Mean =-5.328 mm, Std Dev. = 1.947 mm, Transducer Diameter = 5.080 mm.

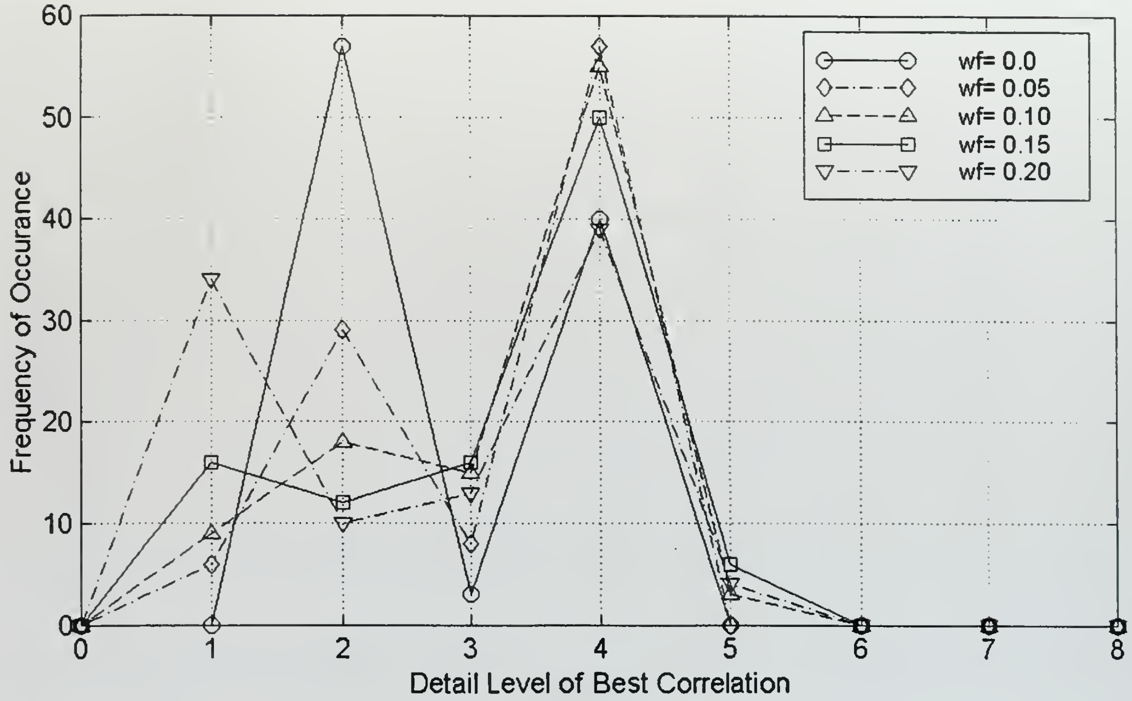

Figure B.31. Histogram of Detail Level of Best Crosscorrelation Small Steel Rod Signals 01 through 100, Sensors #1 and #2, min.(variance/max.), weighting factor = [0.0, 0.05, 0.10, 0.15, 0.20]

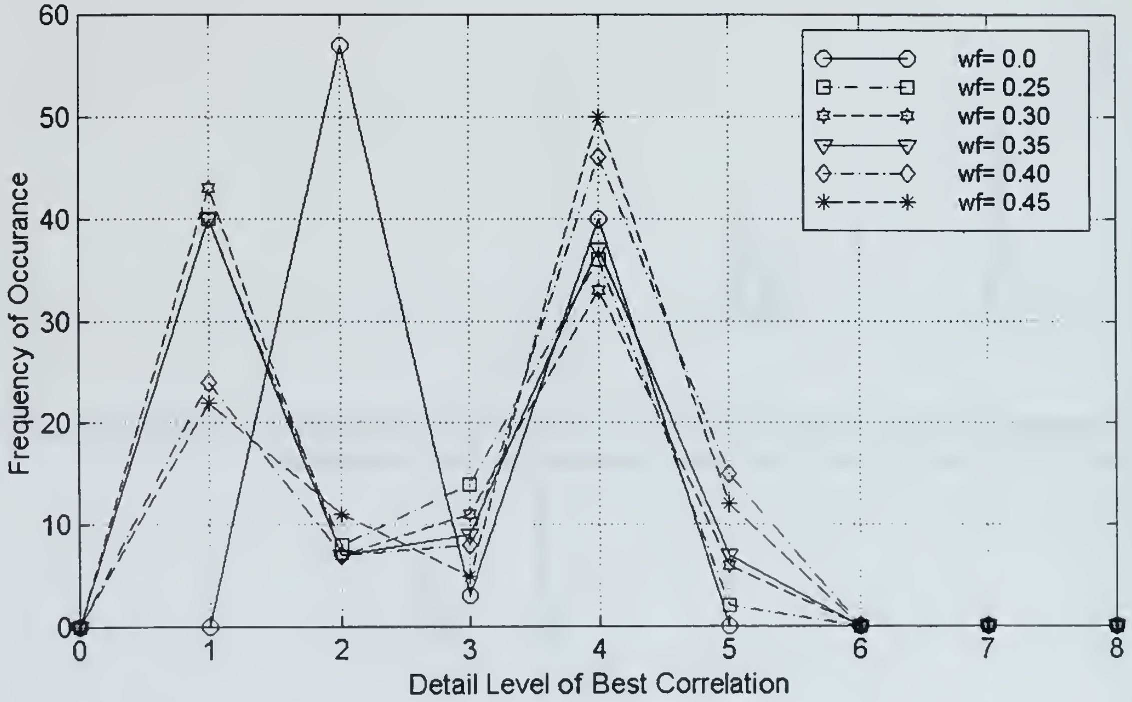

Figure B.32. Histogram of Detail Level of Best Crosscorrelation Small Steel Rod Signals 01 through 100, Sensors #1 and #2, min.(variance/max.), weighting factor = [0.0, 0.25, 0.30, 0.35, 0.40, 0.45]

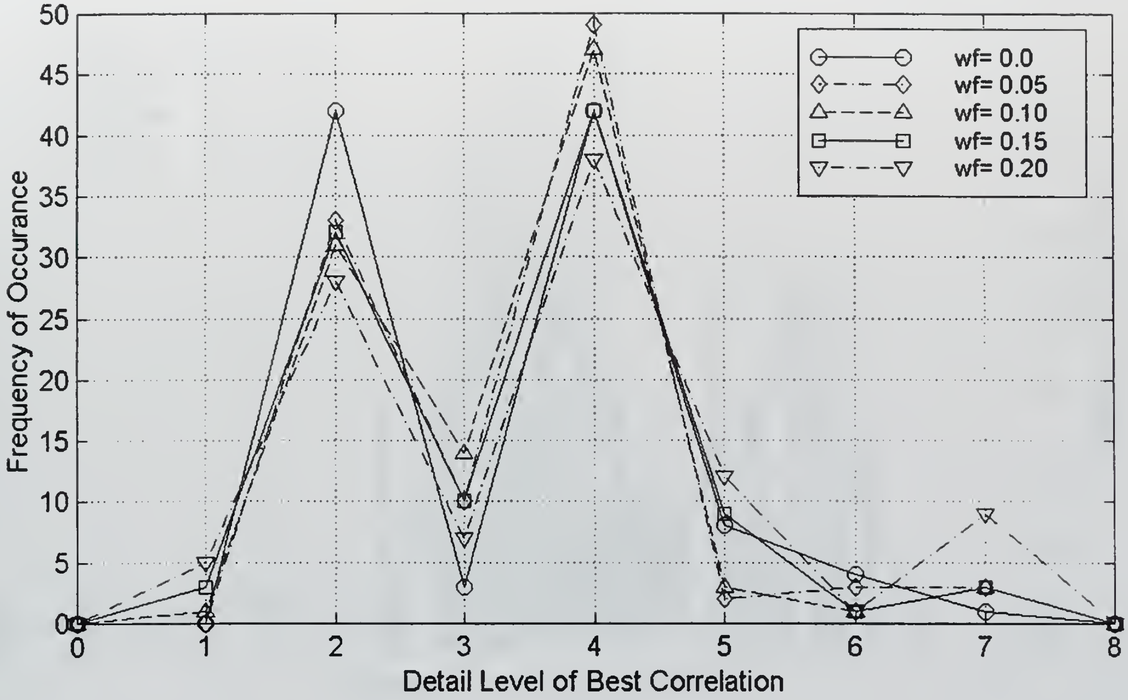

Figure B.33. Histogram of Detail Level of Best Crosscorrelation Small Steel Rod Signals 01through 100, Sensors #1 and #3, min.(variance/max.), weighting factor = [0.0, 0.05, 0.10, 0.15, 0.20]

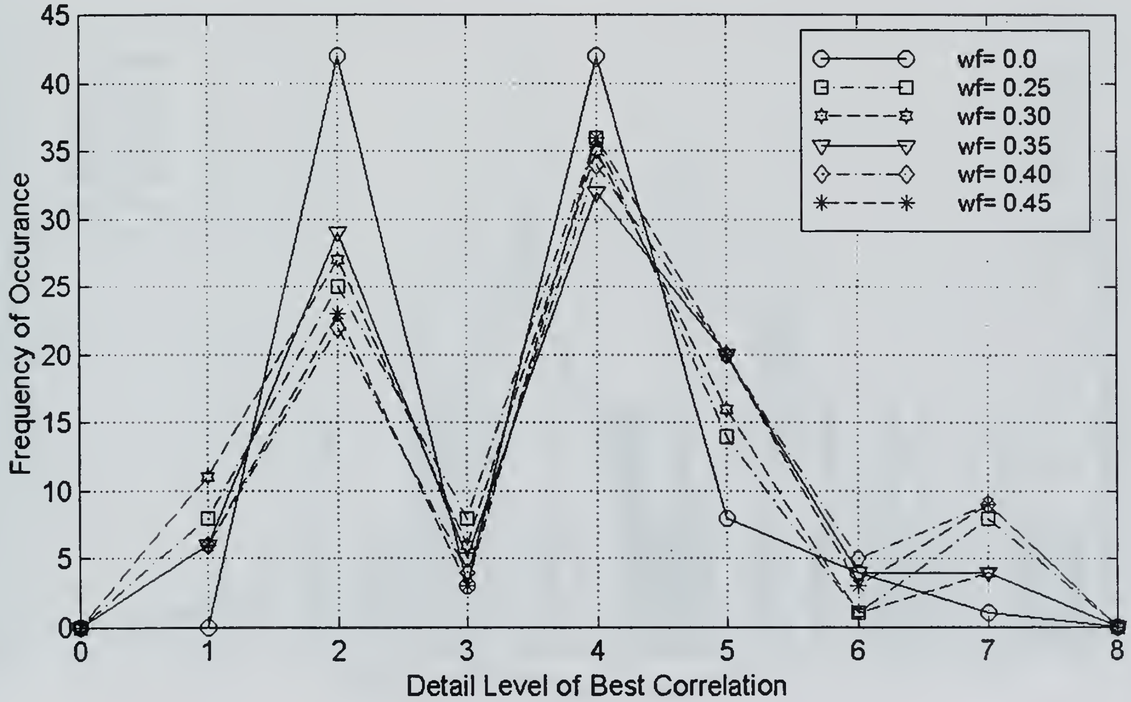

Figure B.34. Histogram of Detail Level of Best Crosscorrelation Small Steel Rod Signals 01 through 100, Sensors #1 and #3, min.(variance/max.), weighting factor = [0.0, 0.25, 0.30, 0.35, 0.40, 0.45]

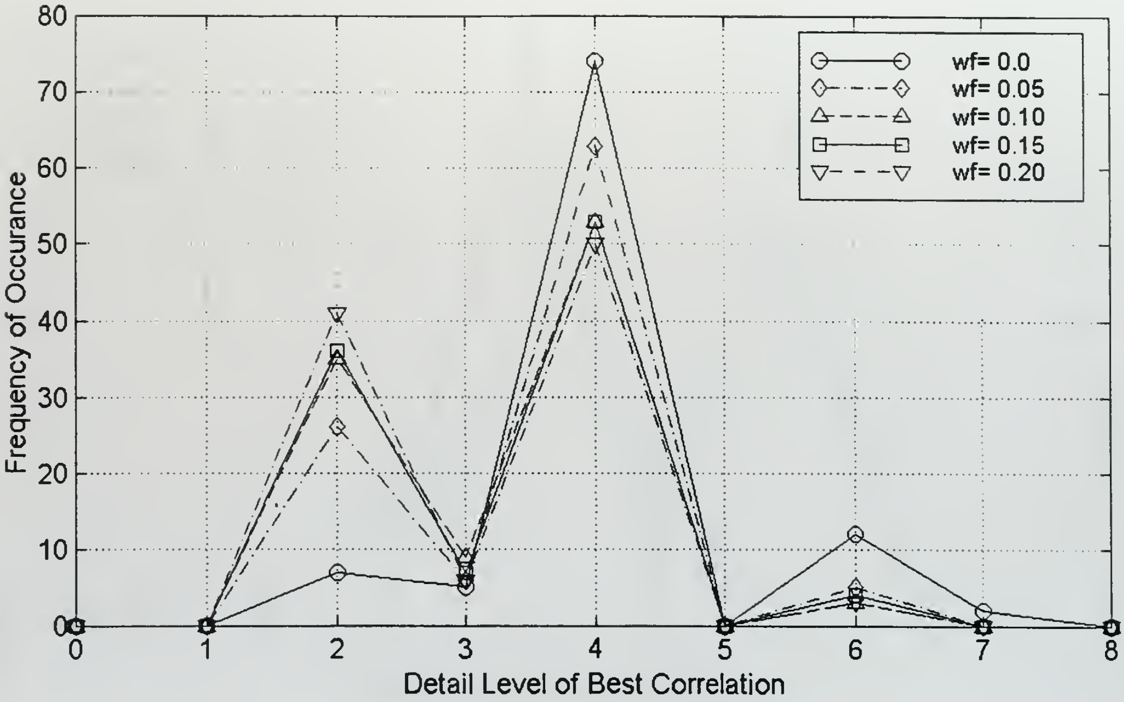

Figure B.35. Histogram of Detail Level of Best Crosscorrelation Small Steel Rod Signals 01through 100, Sensors #1 and #4, min.(variance/max.), weighting factor = [0.0, 0.05, 0.10, 0.15, 0.20]

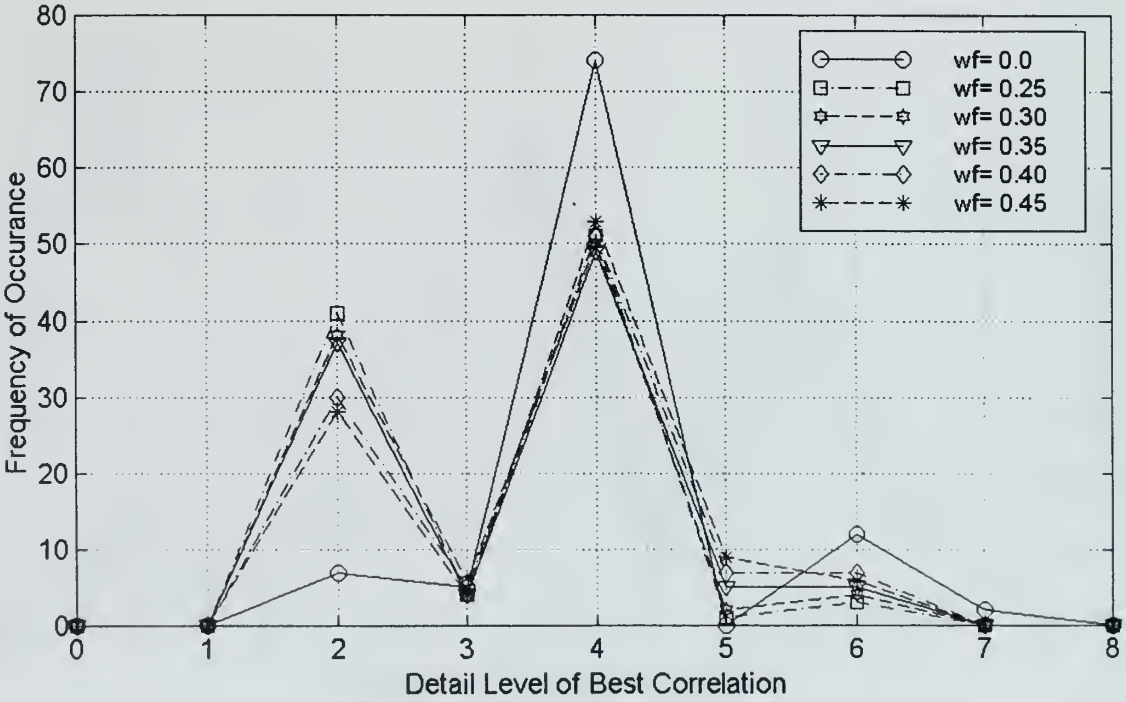

Figure B.36. Histogram of Detail Level of Best Crosscorrelation Small Steel Rod Signals 01 through 100, Sensors #1 and #4, min.(variance/max.), weighting factor = [0.0, 0.25, 0.30, 0.35, 0.40, 0.45]

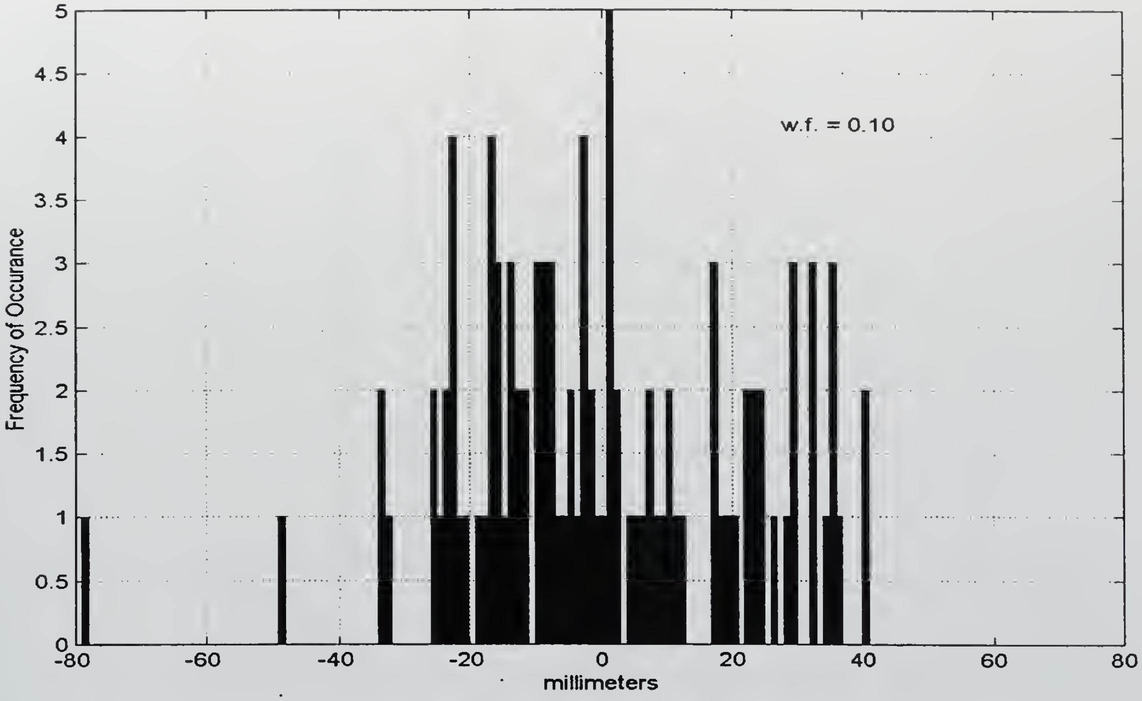

Figure B.37. Wavelet Detail Crosscorrelation Location Histogram for Small Steel Rod Sensors #1 and #2, Mean = -0.008 mm, Std Dev. = 21.470 mm, Transducer Diameter = 5.080 mm.

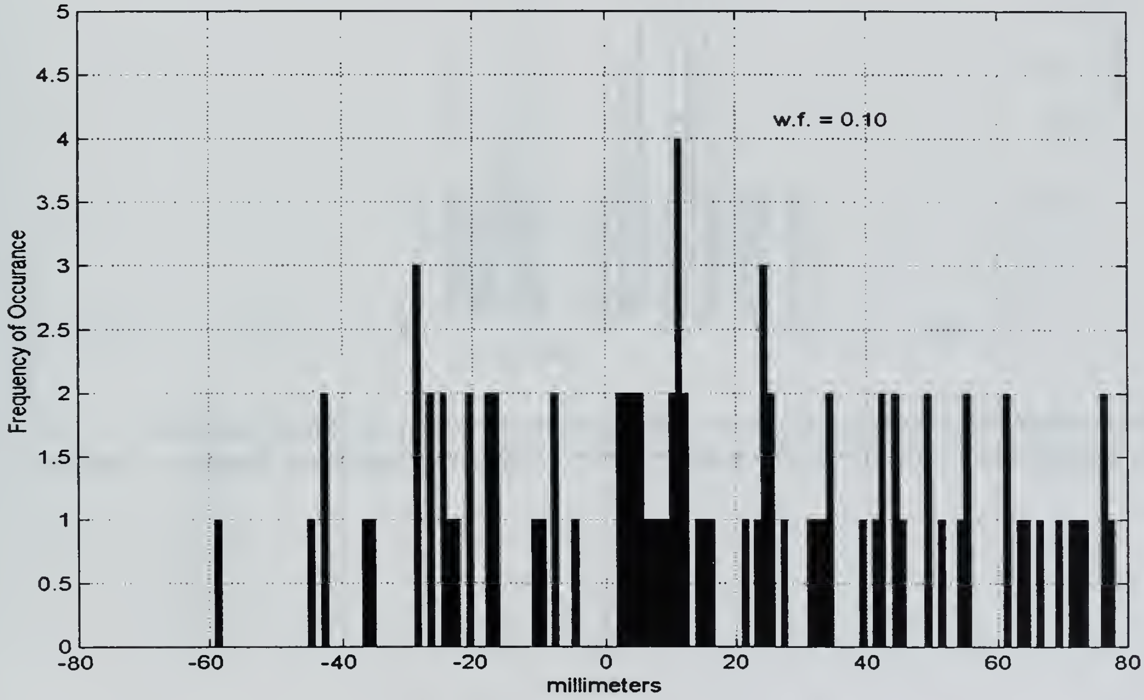

Figure B.38. Wavelet Detail Crosscorrelation Location Histogram for Small Steel Rod Sensors #1 and #3, Mean = 23.281 mm, Std Dev. = 43.284 mm, Transducer Diameter = 5.080 mm.

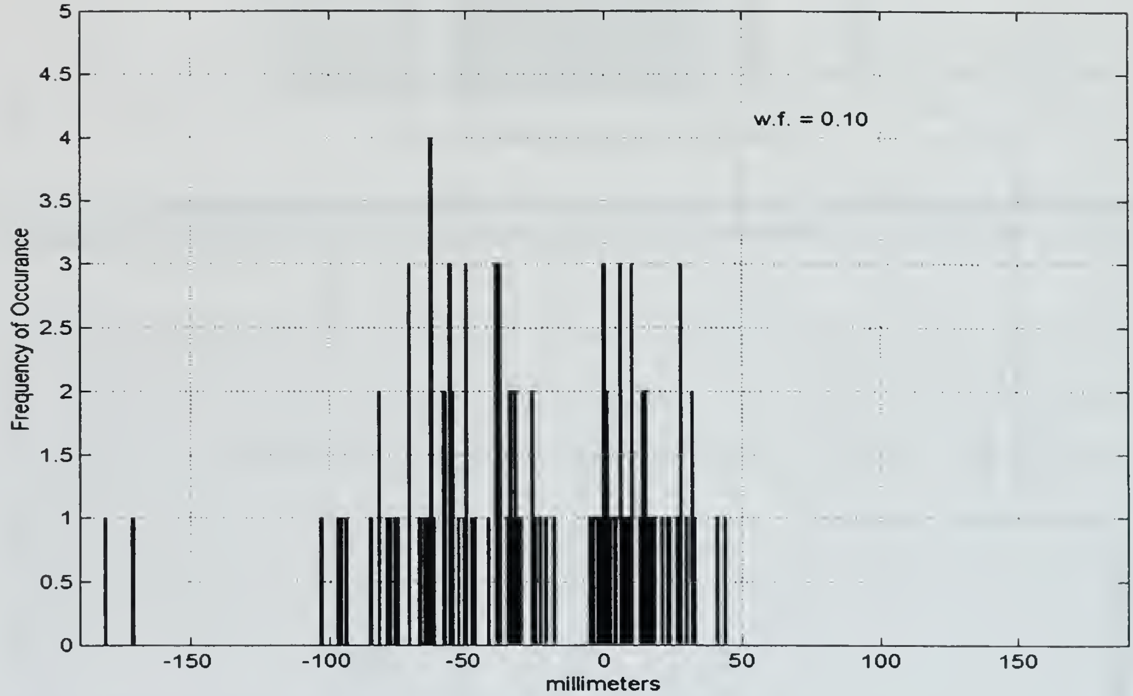

Figure B.39. Wavelet Detail Crosscorrelation Location Histogram for Small Steel Rod Sensors #1 and #4, Mean = -28.541 mm, Std Dev. = 43.473 mm, Transducer Diameter = 5.080 mm.

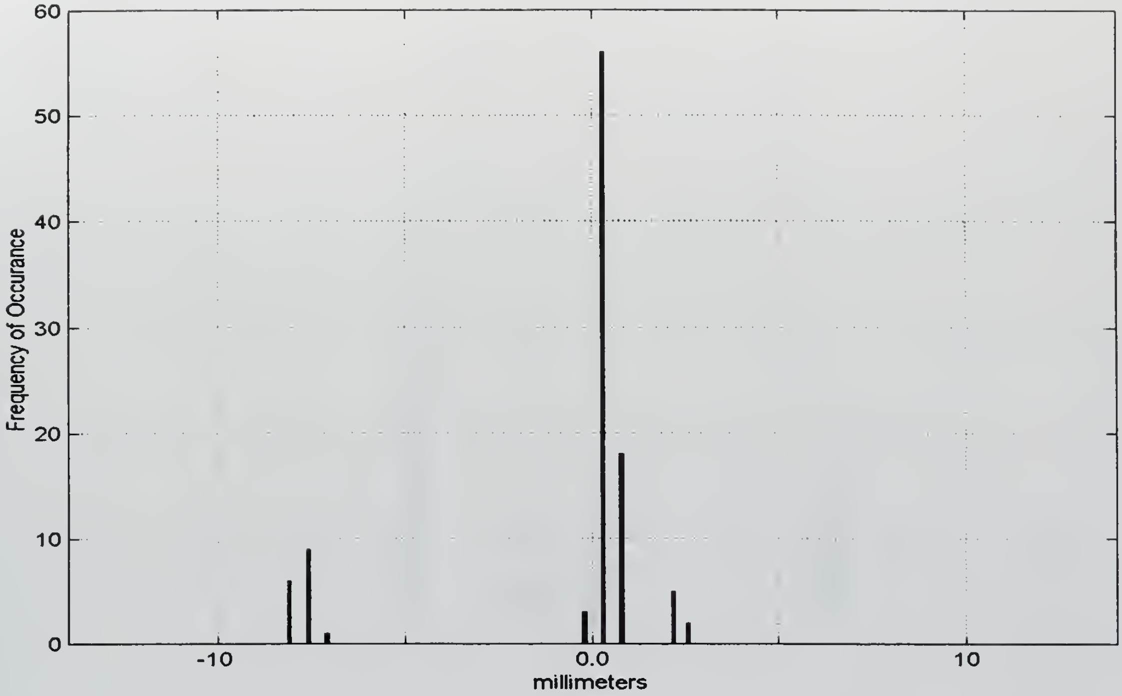

Figure B.40. Threshold Crossing Location Histogram for Carbon Fiber Rod Sensors #1 and #2 Mean = -0.773 mm, Std Dev. = 3.112 mm, Transducer Diameter = 5.080 mm.

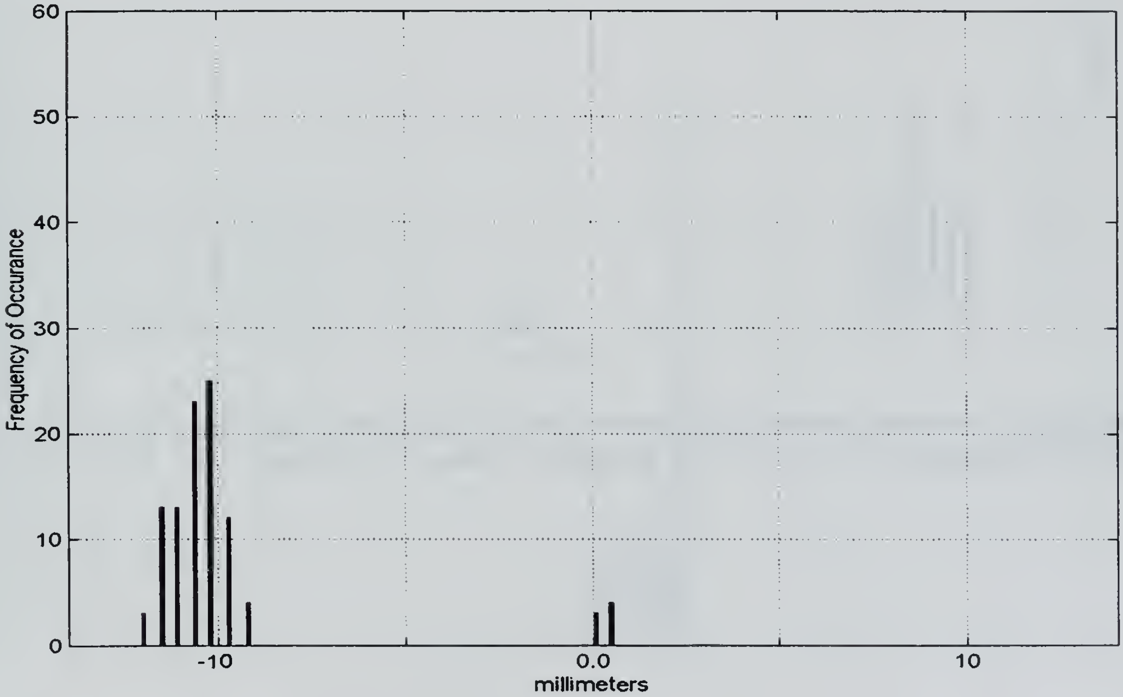

Figure B.41. Threshold Crossing Location Histogram for Carbon Fiber Rod Sensors #1 and #3 Mean = -9.795 mm, Std Dev. = 2.865 mm, Transducer Diameter = 5.080 mm.

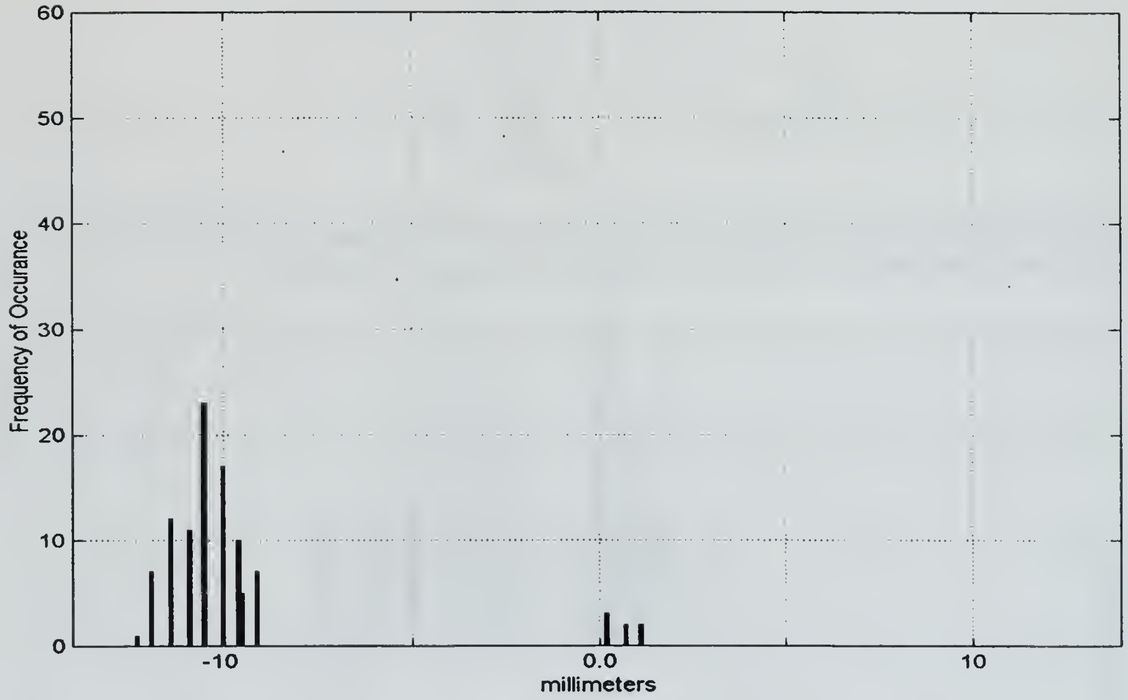

Figure B.42. Threshold Crossing Location Histogram for Carbon Fiber Rod Sensors #1 and #4 Mean = -9.668 mm, Std Dev. = 2.937 mm, Transducer Diameter = 5.080 mm.

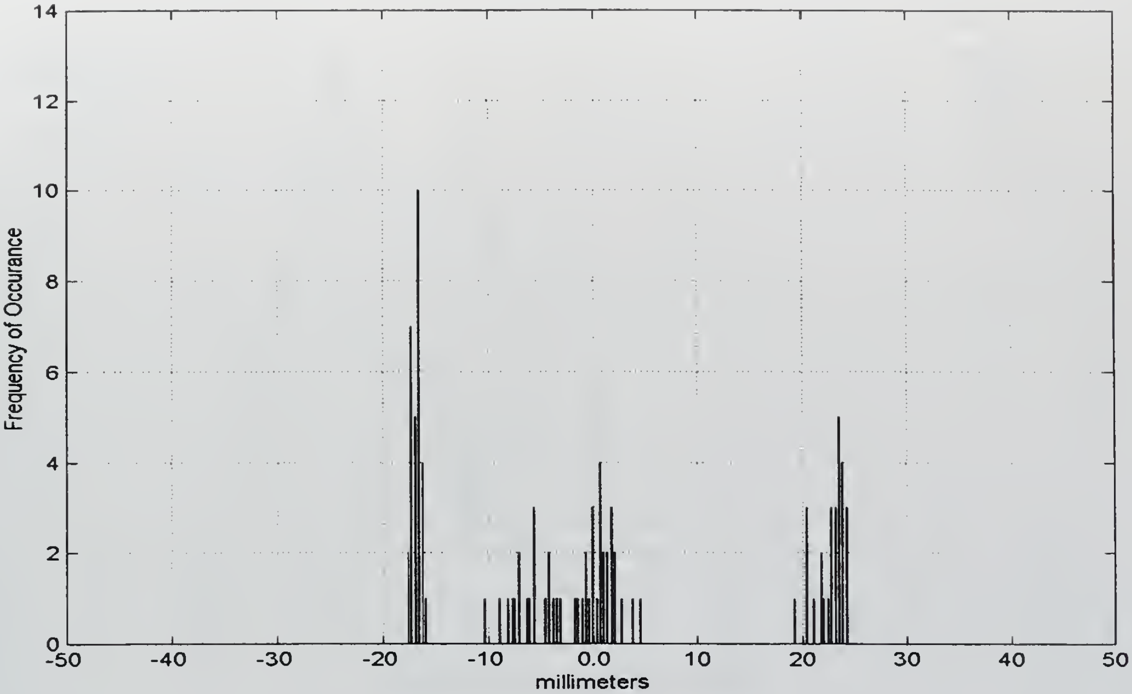

Figure B.43. Gaussian Crosscorrelation Location Histogram for Carbon Fiber Rod Sensors #1 and #2 Mean = 0.344 mm, Std Dev. = 15.212 mm, Transducer Diameter = 5.080 mm.

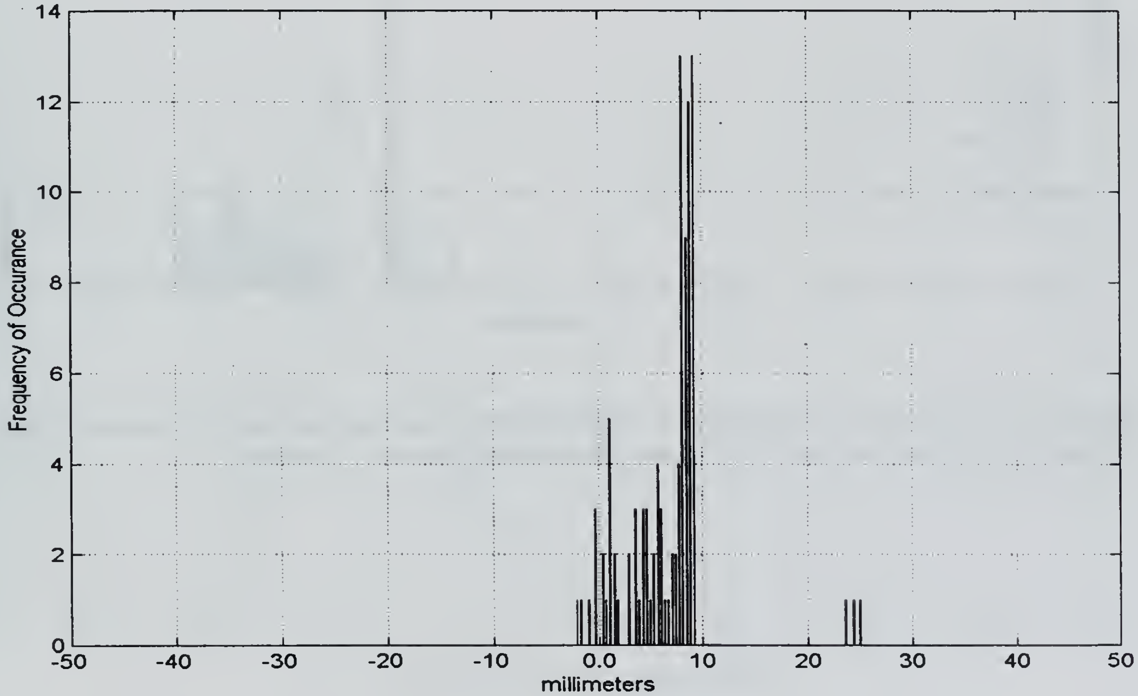

Figure B.44. Gaussian Crosscorrelation Location Histogram for Carbon Fiber Rod Sensors #1 and #3 Mean = 7.174 mm, Std Dev. = 6.514 mm, Transducer Diameter =5.080 mm.

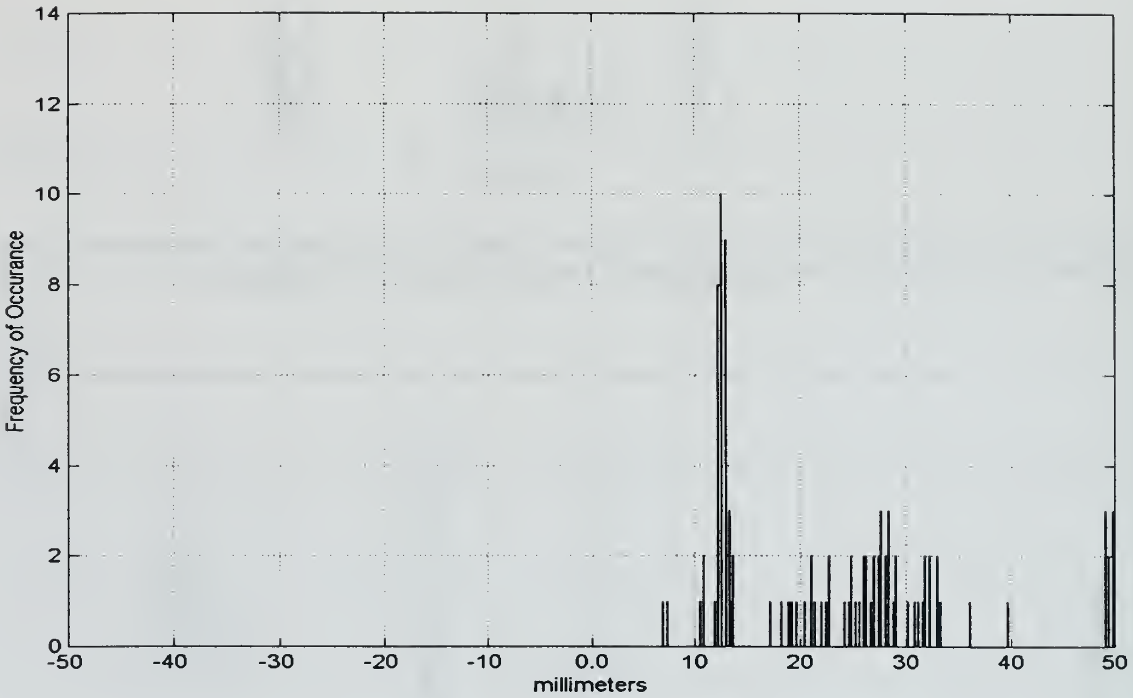

Figure B.45. Gaussian Crosscorrelation Location Histogram for Carbon Fiber Rod Sensors #1 and #4 Mean =22.825 mm, Std Dev. = 11.505 mm, Transducer Diameter = 5.080 mm.

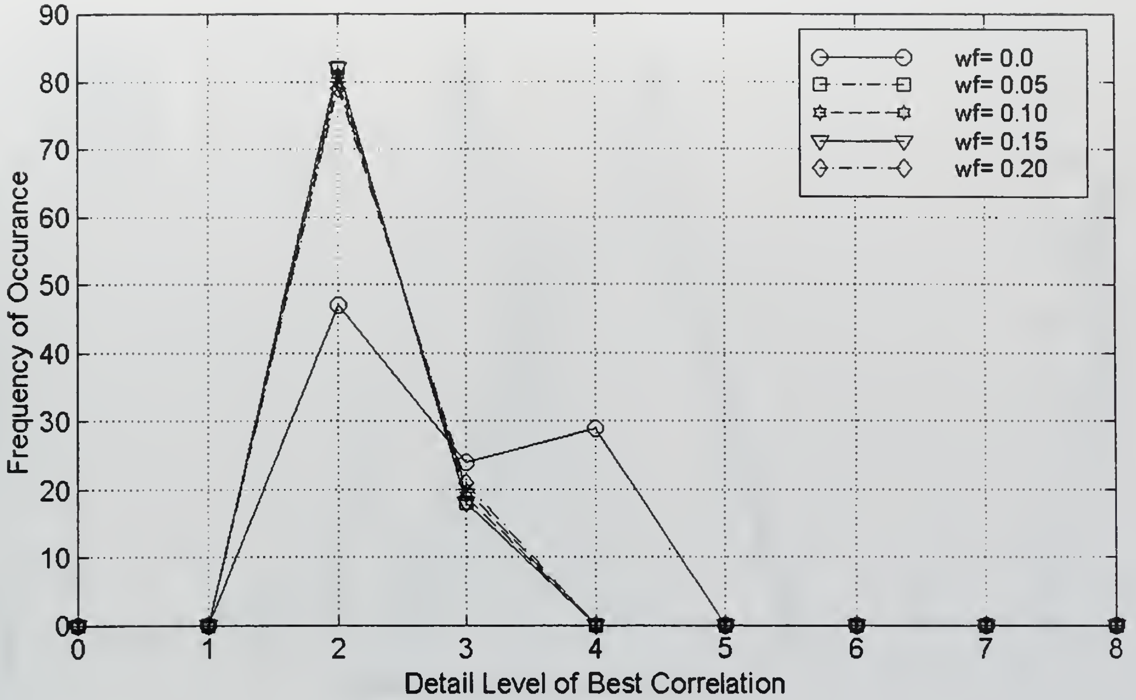

Figure B.46. Histogram of Detail Level of Best Crosscorrelation Carbon Fiber Rod Signals 01 through 100, Sensors #1 and #2, min.(variance/max.), weighting factor = [0.0, 0.05, 0.10, 0.15, 0.20]

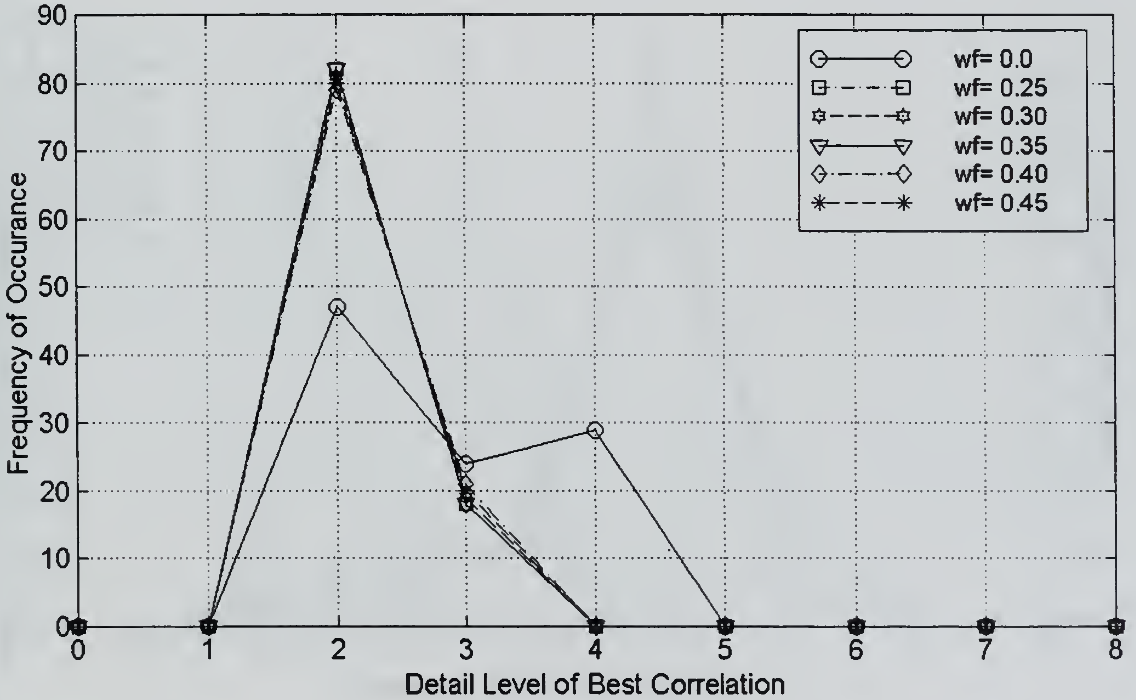

Figure B.47. Histogram of Detail Level of Best Crosscorrelation Carbon Fiber Rod Signals 01 - 100, Sensors #1 and #2, min.(variance/max.), weighting factor =[0.0, 0.25, 0.30, 0.35, 0.40, 0.45]

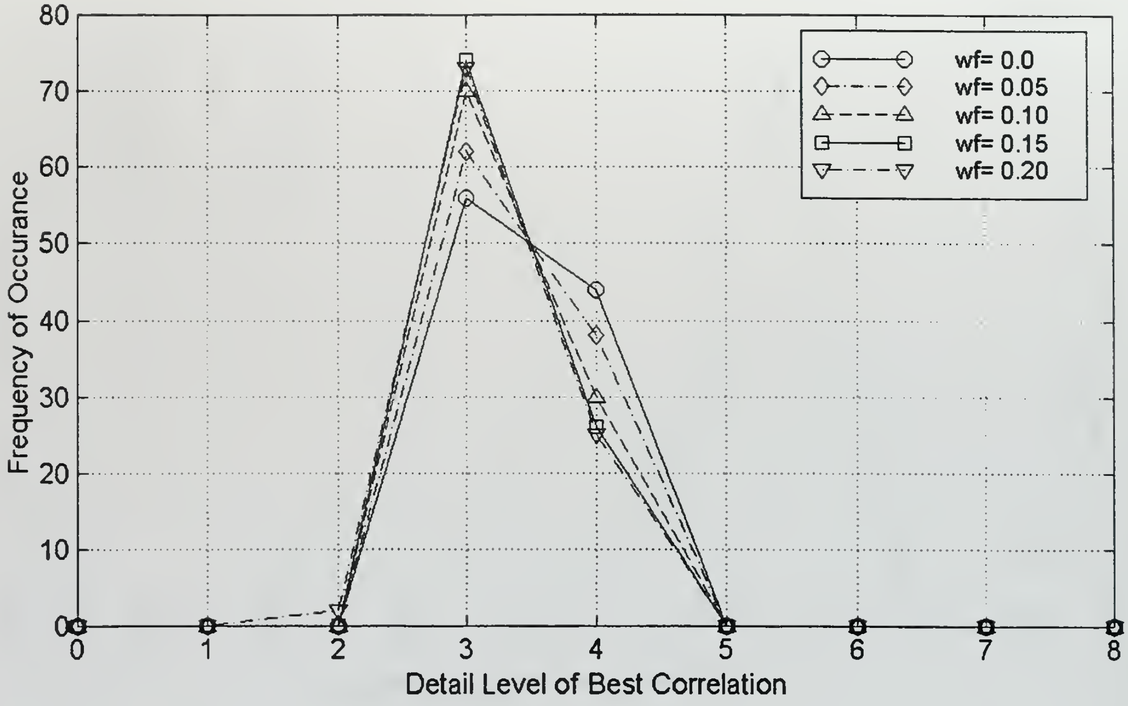

Figure B.48. Histogram of Detail Level of Best Crosscorrelation Carbon Fiber Rod Signals 01 - 100, Sensors #1 and 33, min.(variance/max.), weighting factor = [0.0, 0.05, 0.10, 0.15, 0.20]

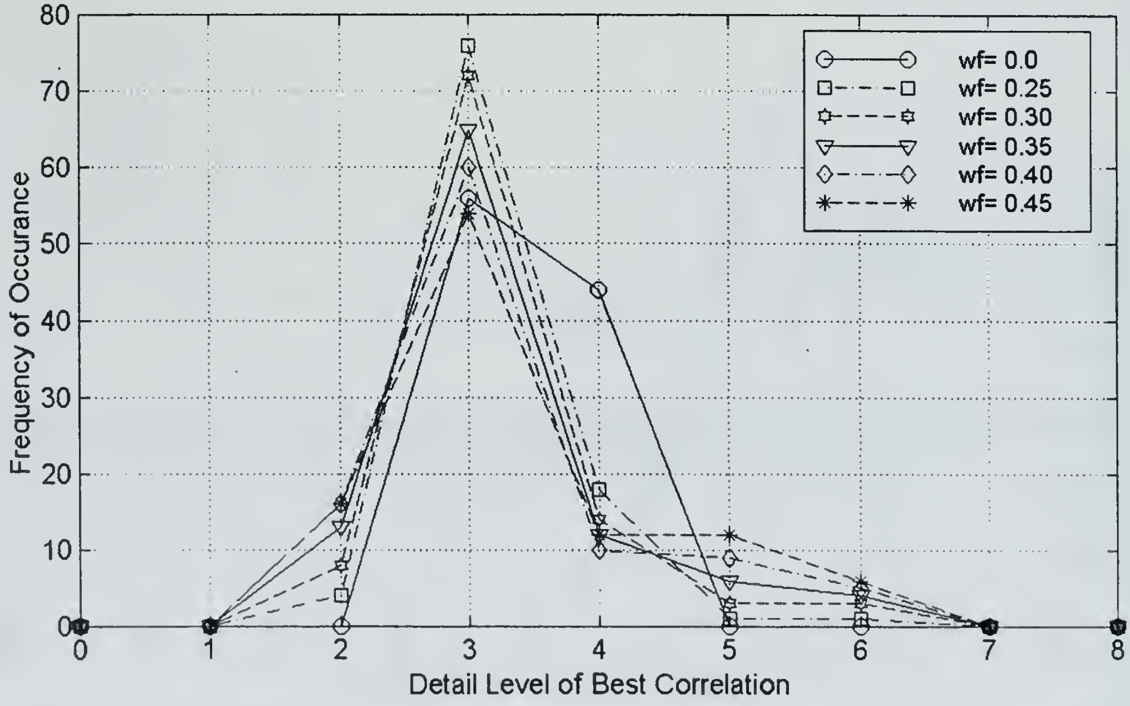

Figure B.49. Histogram of Detail Level of Best Crosscorrelation Carbon Fiber Rod Signals 01 - 100, Sensors #1 and 33, min.(variance/max.), weighting factor =[0.0, 0.25, 0.30, 0.35, 0.40, 0.45]

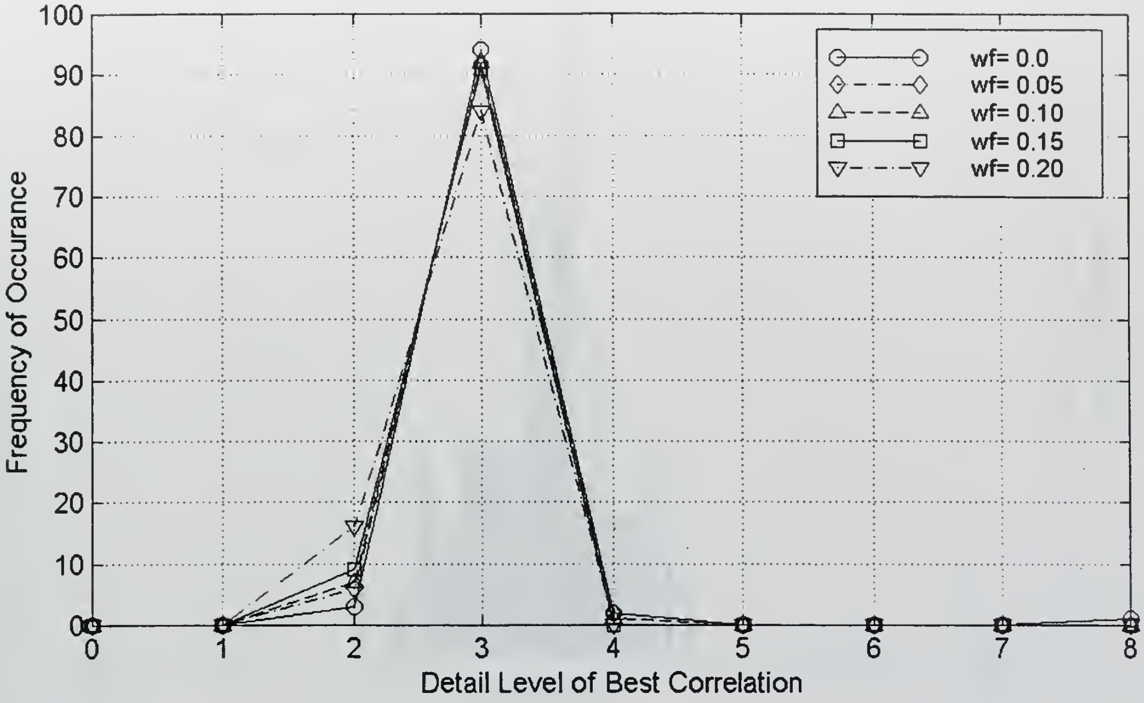

Figure B.50. Histogram of Detail Level of Best Crosscorrelation Carbon Fiber Rod Signals 01 - 100, Sensors #1 and #4, min.(variance/max.), weighting factor = [0.0, 0.05, 0.10, 0.15, 0.20]

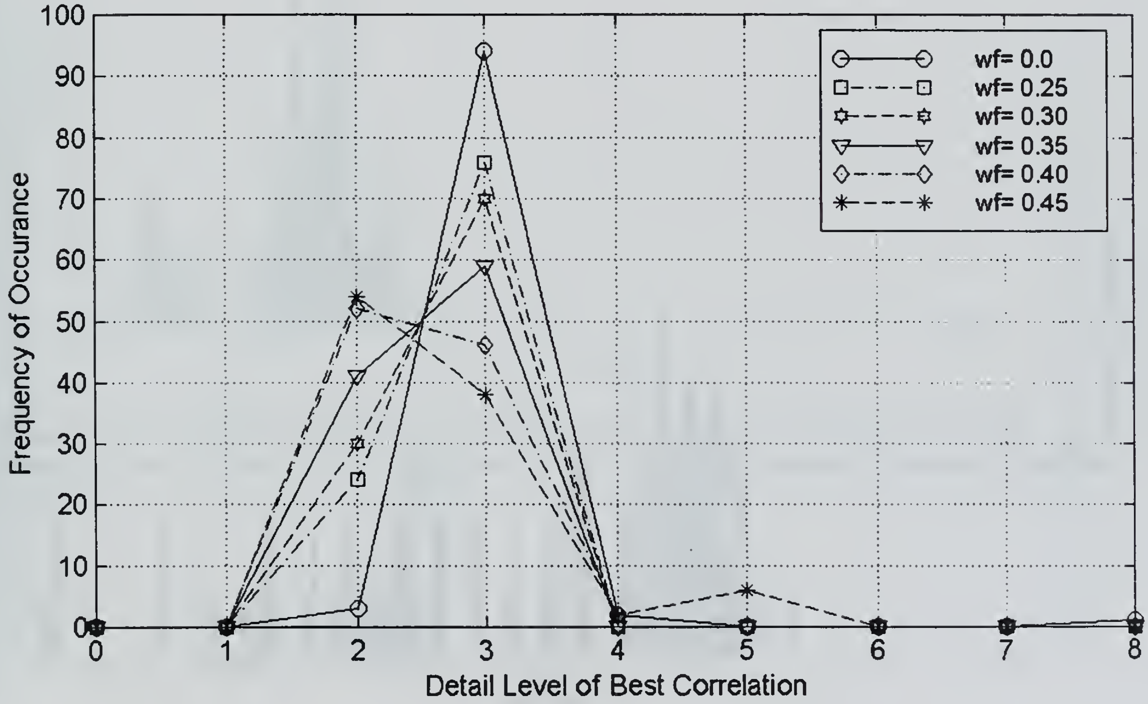

Figure B.51. Histogram of Detail Level of Best Crosscorrelation Carbon Fiber Rod Signals 01 - 100, Sensors #1 and 34, min.(variance/max.), weighting factor =[0.0, 0.25, 0.30, 0.35, 0.40, 0.45]

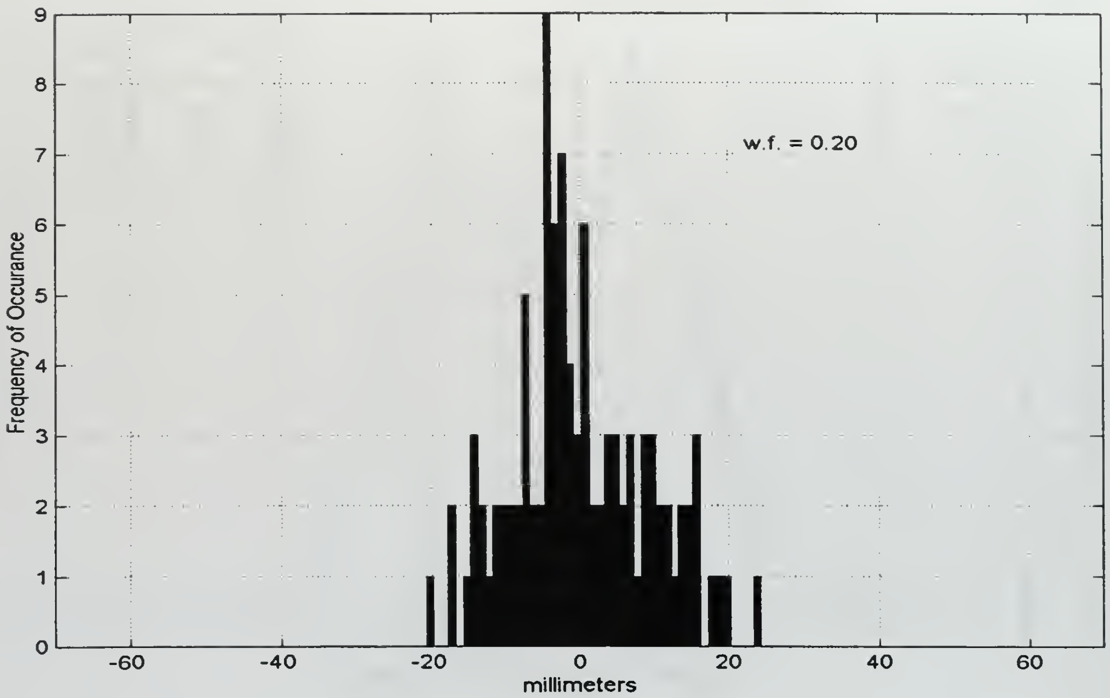

Figure B.52. Wavelet Detail Crosscorrelation Location Histogram for Carbon Fiber Rod Sensors #1 and #2, Mean = 0.000 mm, Std Dev. = 9.281 mm, Transducer Diameter = 5.080 mm.

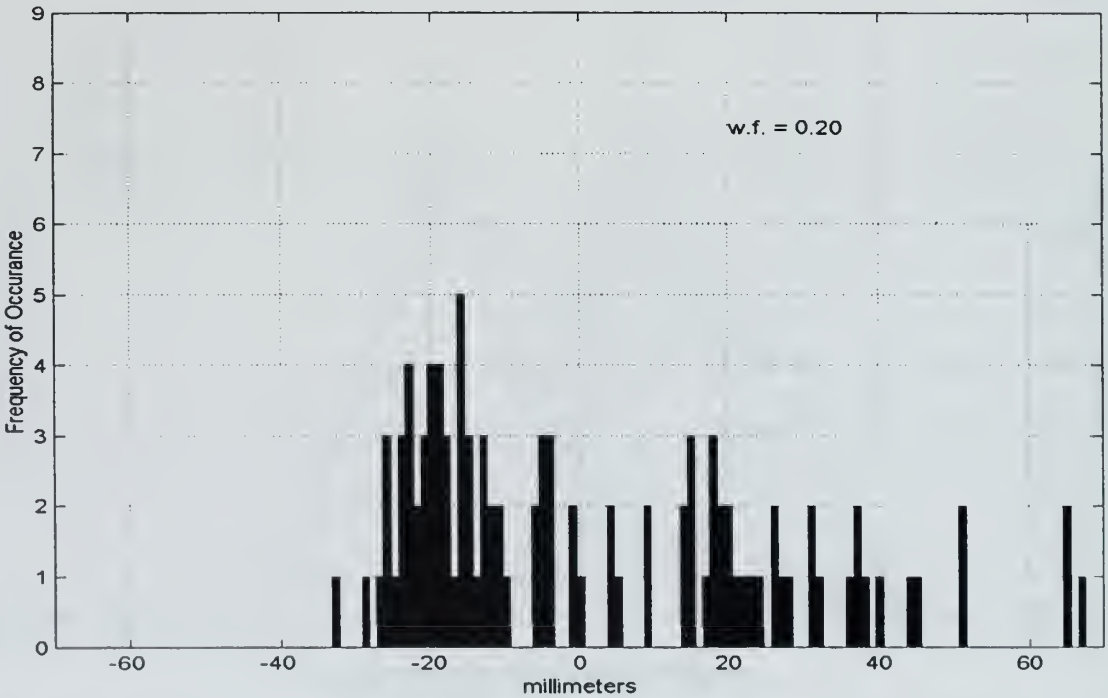

Figure B.53. Wavelet Detail Crosscorrelation Location Histogram for Carbon Fiber Rod Sensors #1 and #3, Mean = 1.726 mm, Std Dev. = 24.617 mm, Transducer Diameter = 5.080 mm.

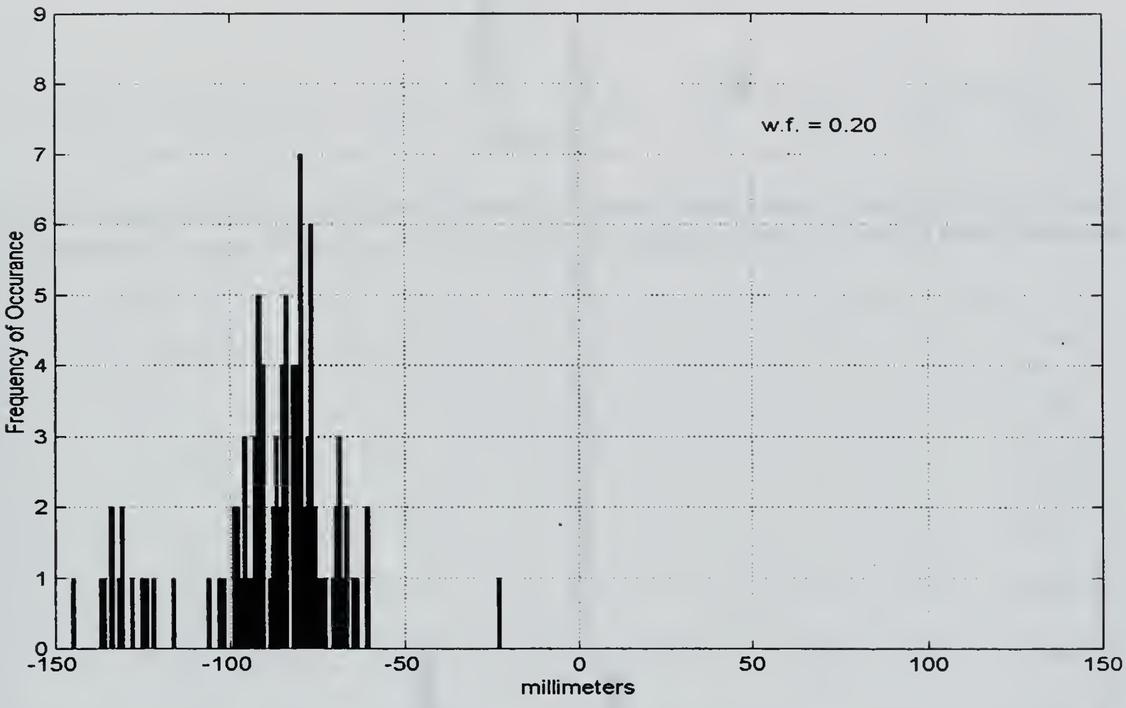

Figure B.54. Wavelet Detail Crosscorrelation Location Histogram for Carbon Fiber Rod Sensors #1 and #4, Mean = -88.572 mm, Std Dev. = 19.861 mm, Transducer Diameter = 5.080 mm.

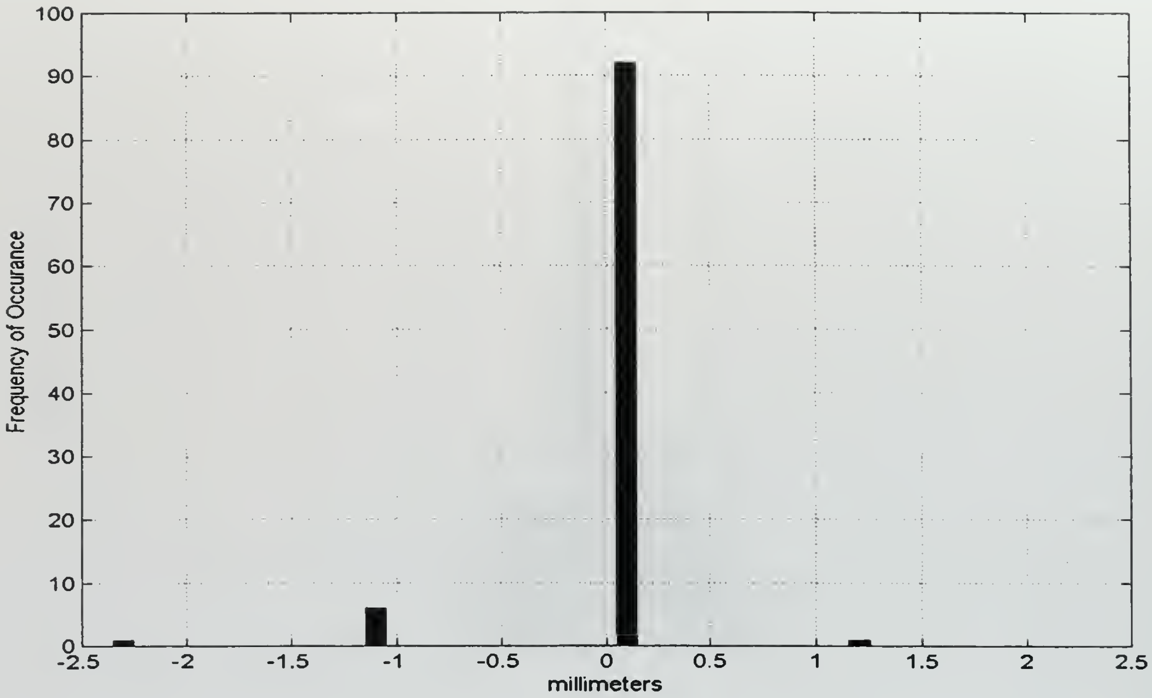

Figure B.55. Windowed Wavelet Detail Crosscorrelation Location Histogram for Carbon Fiber Rod Sensors #1 and #2, Mean = 0.000 mm, Std Dev. = 0.388 mm, Transducer Diameter = 5.080 mm.

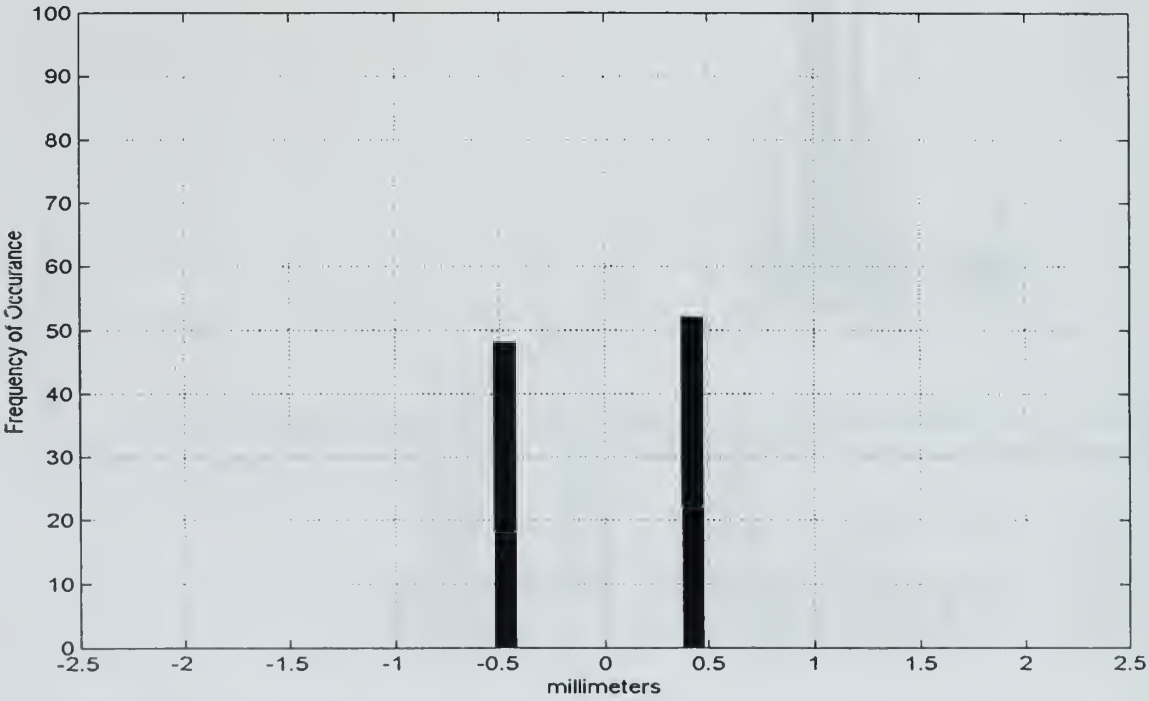

Figure B.56. Windowed Wavelet Detail Crosscorrelation Location Histogram for Carbon Fiber Rod Sensors #1 and #3, Mean = 0.000 mm, Std Dev. = 0.459 mm, Transducer Diameter = 5.080 mm.

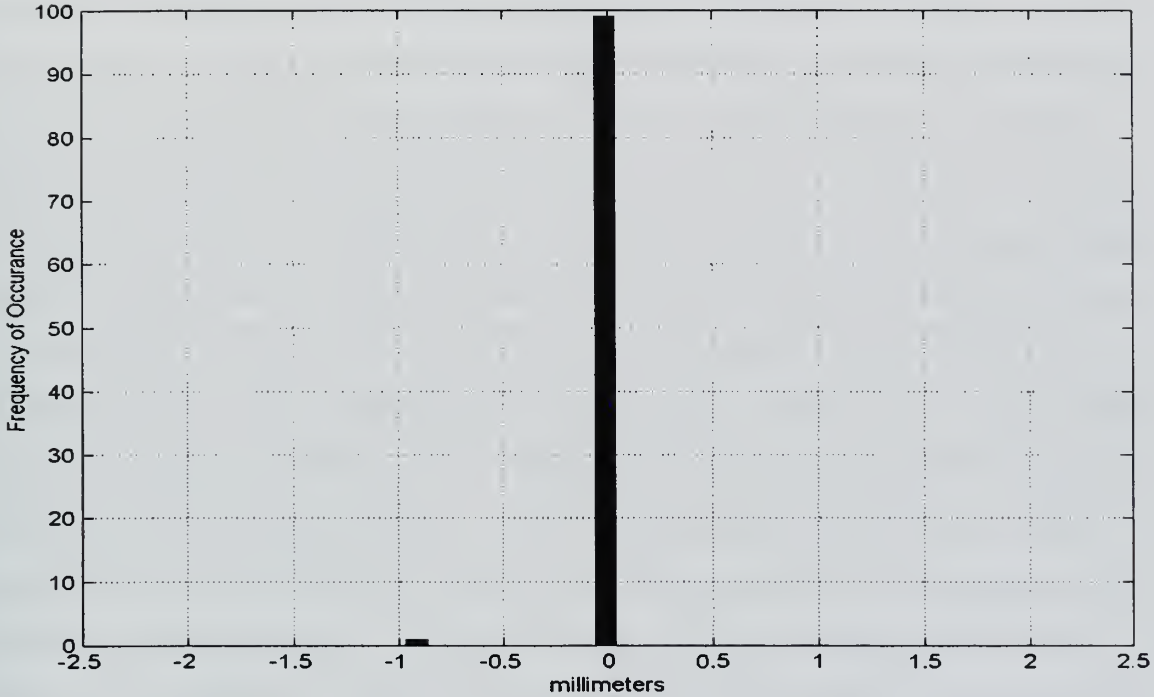

Figure B.57. Windowed Wavelet Detail Crosscorrelation Location Histogram for Carbon Fiber Rod Sensors #1 and #4, Mean = 0.000 mm, Std Dev. = 0.092 mm, Transducer Diameter = 5.080 mm.

APPENDIX C. EXPERIMENTAL METHODS

A. MAKING TEST SIGNALS

The Fracture Wave Detector hardware is set up in accordance with the FWD users guide. The step by step instructions are thorough and complete. If the specimen is not connected, begin with the large steel rod. Place the rod on the testing bench, and slide the for large transducer holders over the rod. Put the transducer holders on the rod where you want them. Place a small amount of silicon vacuum grease on each of the transducers and gently place them into the holders until the face of the transducer touches the test rod. Put a dental rubber band over the top, and attach it to the pins in the side of the transducer holders. Ensure that the rubber band lies over the top of the transducer. If two rubber bands are tied together to form a figure eight, two sets of them will maintain the contact force, and the rubber band will last longer. The large transducers and holders are sturdier than the small transducers, so they should be used until the system is familiar to the user. Connect the transducers to the preamplifiers, and the preamplifiers to the filter Trigger Modules. Verify the switch settings on the Filter Trigger Modules. The total gain should be in the range of 41 decibels to start. If the gain on the preamplifiers is 20 db, the gain *switch* on each FTM should be up, to +21 db. The gain *knob* should be fully counter-clockwise to 0 db. Double check that all four preamplifiers and all four channel on the FTM have identical settings. The filter and trigger settings are set per the FWD users guide. Plug all the power cords into a power strip, and use the switch on the power strip to turn the system on and off. The FWD hardware needs to be turned on with the computer to work properly. Acquisition of signals should be accomplished in DOS mode. The post test and location procedures may be done in Windows. When the computer finishes booting up, go the start button and select shut down. At the shut down window

toggle the radio button to "Restart in MS DOS Mode", and select OK. At the DOS prompt, change to the FWD directory by typing

C:\ cd fwd12 <return>

which will come back as

C:\FWD12\ <return>

to execute the FWD software, type

FWD96 <return>

The FWD12 window will now appear. If this is the first time using the module, take a hour to read the users guide, it will pay off in the long term. Use the mouse to select the acquisition module. Select setup and verify the settings. The pre-trigger setting should be 12.5%, the memory length 2048, and the digitization rate 10 Mhz. Check the four channel mode button, and select OK. The parametric settings are used only if there is a forcing function applied to the test specimen. Select start from the acquisition window. The window will now fill with the plot windows. Take the Pentel 0.3 mm pencil with H lead. Click five or six times on the end to extend the lead. Place the lead gently on the test specimen where the signal will originate. Hold the pencil at 30 to 45 degrees to the test surface, and increase force until the lead breaks. The trigger lights should flash, and the waveforms appear on the data windows. If there is only going to be one event per data file, select end, and name the file. Exit the acquisition module. And enter the post test module. The use of the location module is explained in the FWD users guide. In order to use the signal in MATLAB, in will need to be converted to tab delimited ASCII text. In the post test module, select File, and open the file that you just saved. On the menu bar select Export, select ASCII Text file type, retype the desired file name in the window, and hit OK. The file name will have a .txt extension automatically. Exit the post test module, and Quit the FWD program. This will return the computer to DOS. Type WIN to restart Windows. Start Excel, and open the file that was just saved. The file will have a .txt, so ensure that Excel is looking for text file types. The file will come

in as comma delimited text, and the program will step you through that. The data will be in five columns. The first column is the time, and the second through fifth columns are the signals from sensors one, two, three, and four respectively. Select Save As, and select Tab Delimited Text. The .txt extension needs to be changed to a .mat extension in order for MATLAB to read it. The file should be saved in the MATLAB directory. Exit Excel and start MATLAB. If the time column is unneeded, delete the column in Excel. The signal can be loaded into MATLAB by using the command

>> load *filemane.mat* -ascii

The MATLAB script files used in this thesis are in Appendix C. To plot the signals, wavelet decomposition's and crosscorrelation functions, use *signal_plotter.m*

APPENDIX D. MATLAB SCRIPT FILES

A. WAVEDETXCORR.M

```
%%%%%%%%%%%%%%%%%%%%%%%%%%%%%%%%%%%%%%%%%%%%%%%%%%%%%%%%%%%%%%%%%%%%%%
%     WAVEDETXCOR = Wavelet Detail Cross Correlation
%     Thesis1.m modified 2-20-98 to window the reconstructed details
%     from the left at the arrival of the longitudinal wave applied
%     to all levels, then from the left at the arrival of the Long.
%     and Trans. waves, finally window the detail levels which contain
%     the long. wave from the left by the long. arrival, and from the
%     right by the trans. wave arrival time, based on the theoretical
%     wave velocities.
clear;
format compact,format long g;
dataload_c;% data file of all the carbon fiber signals
location_window=zeros(100,8,3);%(100,3,10)
%%%%%%%%%%%%%%%%%%%%%%%%%%%%%%%%%%%%%%%%%%%%%%%%%%%%%%%%%%%%%%%%%%%%%%
%     Variable Input
k1=input('What point does the left window start?  ');
k2=input('What point does the right window end?  ');
windowed_signal=signal_setC(k1:k2,:,:);
for z=1:100% Input as 2048 pts
  [data sensor signal]=size(windowed_signal(:,:,z));
  dec_level=8;
  D=zeros(data,dec_level,sensor);
  Xcorl_0=zeros((2*data)-1,dec_level,(sensor-1));
%%%%%%%%%%%%%%%%%%%%%%%%%%%%%%%%%%%%%%%%%%%%%%%%%%%%%%%%%%%%%%%%%%%%%%
  %     Wavelet Decomposition
  for k=1:sensor
     [C(:,k,z),L]=wavedec(windowed_signal(:,k,z),dec_level,'db4');
  end
  %%%%%%%%%%%%%%%%%%%%%%%%%%%%%%%%%%%%%%%%%%%%%%%%%%%%%%%%%%%%%%%%%%%%%%
  %     Detail Reconstruction  D(i,j,k)=detail(1:2048,level,sensor#)
  for k=1:sensor
     for j=1:dec_level
        D(:,j,k)=wrcoef('d',C(:,k,z),L,'db4',j);
        %D(:,j,k)=D_temp(k1:data,j,k);%sets the window on each
        %detail level at the arrival of the long. wave at the trigger.
     end
  end
  %%%%%%%%%%%%%%%%%%%%%%%%%%%%%%%%%%%%%%%%%%%%%%%%%%%%%%%%%%%%%%%%%%%%%%
  %     Detail Cross Correlation
  % Xcorl(i,j,k)=Cross Correlation at each Detail level, j, between
  % Sensor 1 and the other three sensors, k.
  %      l = correlation # 1=1:2; 2=1:3; 3=1:4;
z
```

```
   subplot(dec_level,1,1),plot(Xcorl_0(:,1,k)),grid on,hold on
   plot([0 4095],[fac(1,k) fac(1,k)],'r')
   title(['Sensor 1 Cross Correlated with Sensor',SN,',Detail Level 1'])
   set(gca,'XTickLabel',[' '])
   axis([0 4095 -1 1])
   for j=2:dec_level-1
      DT=int2str(j);
      subplot(dec_level,1,j),plot(Xcorl_0(:,j,k)),grid on,hold on
      plot([0 4095],[fac(j,k) fac(j,k)],'r')
      title(['Detail ',DT])
      set(gca,'XTickLabel',[' '])
      axis([0 4095 -1 1])
   end
   subplot(dec_level,1,dec_level),plot(Xcorl_0(:,dec_level,k)),grid
on,hold on
   plot([MoA_1(dec_level,k) MoA_1(dec_level,k)],[-1 1],'r')
   title(['Detail Level ',DL])
   axis([0 4095 -1 1])
   fig=fig+1;
end  % end of signal_plotter
```

LIST OF REFERENCES

Allen, D.H., Haisler, W.E., *Introduction to Aerospace Structural Analysis*, John Wiley and Sons, 1985.

Chui, C.K., *Wavelets: A Tutorial in Theory and Applications*, Academic Press Inc.,1992.

Cohen, A., Kovacevic, J., *Wavelets: A Mathematical Background*, Proceedings of the IEEE, vol. 84, no. 4, pp. 514-522, April 1996.

Cooper, G.R., McGillem, C.D., *Probabilistic Methods of Signal and System Analysis*, pp. 110-220, Oxford University Press, 1986.

Davies, R.M., *Stress Waves in Solids*, Cambridge Monographs on Mechanics and Applied Mathematics, pp 64-138, Cambridge University Press, 1956.

Daubechies, I., *Ten Lectures on Wavelets*, Society For Industrial and Applied Mathematics, 1992.

Fracture Wave Detector Users Manual, Digital Wave Corporation, March 1996.

Gade, S., Gram-Hansen, K.,*The Analysis of Nonstationairy Signals*, Sound and Vibration, pp. 40-46, January 1997.

Gish, D.A., *Failure Site Location By Acoustic Emission For Composite Reliability Assurance*, Master's Thesis, Naval Postgraduate School, Monterey, California, September 1995.

Hess-Nielsen, N., Wickerhauser, M.V., *Wavelets and Time Frequency Analysis*, Proceedings of the IEEE, vol. 84, no. 4, pp. 523-540, April 1996.

Kolsky, H., *Stress Waves in Solids*, pp. 1-86, Oxford University Press, 1953.

Lurie, R., *Wavelet Analysis Using the MATLAB Wavelet Toolbox*, pp. 1-61, The Mathworks Incorporated, 1996.

Strang, G., Nguyen, T., *Wavelets and Filter Banks*, Wellesley-Cambridge Press, 1996.

Sweldens, W., *Wavelets: What's Next?*, Proceedings of the IEEE, vol. 84, no. 4, pp. 680-685, April 1996.

Ziola, S.M., *Source Location in Thin Plates Using Crosscorrelation*, PhD. Dissertation, Naval Postgraduate School, Monterey, California, December 1991.

INITIAL DISTRIBUTION LIST

1. Defense Technical Information Center 2
   8725 John J. Kingman Rd. STE 0944
   Ft. Belvoir, Virginia 22060-6218

2. Dudley Knox Library 2
   Naval Postgraduate School
   411 Dyer Rd.
   Monterey, California 93943-5101

3. Prof. Gerald H. Lindsey 1
   Code AA/Li
   Department of Aeronautical Engineering
   Naval Postgraduate School
   Monterey, California 93943-5000

4. Prof. Edward M. Wu 3
   Code AA/Wu
   Department of Aeronautical Engineering
   Naval Postgraduate School
   Monterey, California 93943-5000

5. Army Research Office 1
   Engineering and Environmental Science Division
   Post Office Box 12211
   Research Triangle Park, North Carolina 27709-2211
   Attn: Dr. Kailasam Iyer

6. Naval Research Laboratory 1
Mechanics of Materials Branch Code 6380
Washington D.C. 20375
Attn: Dr. Robert Badaliance

7. Army Research Laboratory 1
Bldg 4600
Aberdeen Proving Ground, Maryland 21005-5069
Attn: Dr. S.C. Chou

8. Digital Wave Corporation 1
14 Inverness Drive East
Building B, Suite 120
Englewood, Colorado 80112
Attn: Dr. Steven Ziola

9. LCDR Joseph G. Jerauld 3
5636 Nokomis Drive
La Mesa, California 92041

DUDLEY KNOX LIBRARY
NAVAL POSTGRADUATE SCHOOL
MONTEREY CA 93943-5101

18 483NPG TH 3579
10/99 22527-100

DUDLEY KNOX LIBRARY
3 2768 00366884 9